

I thank the reviewers for valuable comments and constructive critique. All comments were carefully considered and addressed. Answers to all the questions are presented below. Corresponding changes have been made in the revised manuscript.

Comments and answers are numbered according to the Referee number and the order of comment. If changes were made in the revised manuscript, their location (page and lines) are indicated in grey shading in the Reply. In the revised manuscript changes made are marked in red. Figs. 4 and 5 have been re-plotted as recommended. Sections 2 and 3 have been swapped.

While revising I tried to make the presentation more clear and consistent. This resulted in some additional changes which are also marked in red (for these changes no locations are provided in Reply) and one additional simple figure (fig.8).

Referee #1

Comment 1.1

The introduction consists of two very general paragraphs, and does not contain any clear motivation for the study. It is claimed that it is "of interest to analyze [storm FACs'] unique characteristics", but it is not explained why.

Reply to Comment 1.1

The introduction has been extended in order to provide more information on the physical processes related to FACs and to place the present study into context. Motivation for the study has been formulated as follows (p. 3, l. 32 - p.4, ll. 1-7).

"It is the purpose of this paper to characterize the magnitude and position of the large- and smaller scale FACs as their response to the magnetic storm development. The *Swarm* observations are used in order to identify various characteristics of the storm-time FACs for the event of 6–9 September 2017, which was one of the two most severe magnetic storms of the recent solar cycle 24 (the previous event was the St-Patrick storm on 17 March 2015). The September 2017 event is of particular interest because it was a two-step storm during which two major substorms occurred and the FAC system is affected by the storm-substorm interplay. In this paper we investigate the time evolution of the large scale FAC intensities, the displacement of the FAC equatorward boundaries and the extreme small scale currents."

Comment 1.2

The main dataset is the 1 second FAC estimates from *Swarm*. The assumptions involved in deriving this should be clearly described. There are several alternative techniques which could be mentioned, especially techniques that utilize the *Swarm* A-C conjunction. How does the results depend on the choice of technique?

Reply to Comment 1.2

The *Swarm* data base contains FACs computed using as the single-satellite as the dual-satellite approaches. In the present study the single-satellite FACs are used because this technique is identical for all three satellites. Since FACs from A, B and C satellites are used, we need the similar method of derivation for all of them. In general, if the dual-satellite method is applied, the resulted FACs are seem to be slightly weaker, than those obtained by the single-satellite method. The following additions explaining the single-satellite as the dual-satellite approaches have been included to section 2.1 Instrumentation (p. 4, ll. 25-29 - p.5, ll. 1-15).

"FACs are detected by their magnetic perturbations in the orthogonal plane which are obtained after subtracting the main magnetic field model from the total measured values. From single spacecraft the FAC density can be estimated based on one magnetic component with a techniques invoking Ampere's law under assumptions about the infinite current sheet geometry and the orthogonal crossing of the current sheet. This method was used for the previous one-satellite missions, such as Magsat and Ørsted (Christiansen et al., 2002). It is also applied to each *Swarm* satellite separately. The dual-satellite estimation method calculates current density from $\text{curl}(B)$ measured quasi-simultaneously at 4 locations is adapted for SwA and SwC data, where measurements separated along-track are used to create a 'tetrahedron' (Ritter and Lühr, 2006). The $\text{curl}(B)$ method provides more reliable current density estimates, as it does not require any assumptions on current geometry and orientation. The FAC output of both a dual-satellite and a single satellite methods are considered to be in a reasonable agreement (Ritter et al., 2013). However, a high degree of coherence is typical at auroral latitudes, while in the polar cap the results based on dual-spacecraft technique as more reliable (Luhr et al., 2016). Both algorithms

are implemented to generate the *Swarm* products that are produced automatically by ESA's processing center as soon as all input data are available. The products are provided using the dual-satellite method on the lower pair of satellites SwA and SwC, and the single-satellite solution for each of the Swarm spacecraft individually. The 1 s values (1 Hz sampling rate) of FAC densities are available via the on-line *Swarm* data portal (<ftp://swarm-diss.eo.esa.int>) as Level 2 data products (Swarm Level 2 Processing System Consortium, 2012). In the present study the single-satellite FACs are used in order to apply the similar method to SwB and SwA/SwC data.”

Comment 1.3

There are no references where one can find more information about the instruments (not just the magnetometers, plasma measurements are also used in the paper without proper introduction).

Reply to Comment 1.3

More information (including references) about the magnetometers and the plasma probe along with the appropriate references has been added to section 2.1 Instrumentation. The following para describes the mission instruments and provides references.

(p. 4, l. 10-11):

“The ESA Swarm mission is a constellation consisting of the three identical satellites (hereafter SwA, SwB and SwC, respectively), all are at the low-altitude polar orbit (Friis-Christensen et al., 2008).”

....

(p. 4, ll. 21-25):

“The mission has a multi-instrument payload. The main module is the high-sensitivity vector (fluxgate type) and scalar magnetometers for determining the magnitude and direction of the total vector and variations of the geomagnetic field with an accuracy of more than 0.5 nT (Merayo et al., 2008). Magnetometers make it possible to carry out measurements in a wide range, including the Earth's main magnetic field and the variations of external magnetic field generated by FACs.”

.....

(p.5, ll. 17-22):

“Each satellite is also equipped with the Electric Field Instrument which includes the Langmuir probe to provide measurements of ionospheric plasma parameters: electron density, electron temperature and spacecraft potential (Knudsen et al., 2003). The plasma data are available at 2 Hz sampling rate as the standard product of the *Swarm* data base. Unfortunately, due to technical problems, measurements of the electric field and ions are rather rare. Nevertheless, the combination of data provided by a magnetometer and a plasma analyzer on electrons makes it possible to identify perturbations associated with FACs.”

Comment 1.4

It is claimed in the abstract and in the conclusions that R1/R2 currents are composed of small-scale currents. This is never really shown in the data. How do you know that R1/R2 is not a large-scale current system with small-scale currents superimposed?

Reply to Comment 1.4

Fig. 3 shows that the R1/R2 are composed of small-scale currents. This figure depicts the original 1-s FACs (small scale) measured along the track (Fig. 3a), from which large scale currents (Fig. 3.b) are revealed after a smoothing procedure.

Comment 1.5

The word saturation is used to describe the lower limit of the equatorward boundary. It is never explained what is meant. Reference is made to Xiong et al.'s definition, but the data is never presented in such a way that we can compare with how they define it.

Reply to Comment 1.5

To avoid the ambiguity the word "saturation" has been eliminated from the abstract and conclusion. As for the reference to Wang et al. (2006), these authors used the definition "saturation" likely in the sense that the limits of the equatorward boundary were observed not lower than at 50° MLat. In the previous version "saturation" was used in the same sense.

Comment 1.6

In figures 4, 5, and 6, reference is made to external parameters which are shown with rather coarse resolution in Figure 1. It is very difficult to follow the description when one has to go back and forth between the figures to check. It would help to plot SYM-h together with the panels in 4, 5, 6, and also mark the time of substorm onset.

Reply to Comment 1.6

For easier visual comparison the SYM-H and AL have been added to Fig. 4. The SYM-H and substorm onsets have been added to Fig. 5. In Fig. 6 the substorm onsets has been marked.

Comment 1.7

The time of substorm onset is never mentioned in the paper I believe, and this is quite crucial. For example, it is stated that the FACs propagate equatorward during substorms, but you would expect something different: An expansion during the growth phase, and then a contraction. The way that the figures are presented, it is very difficult to see if this is the case.

Reply to Comment 1.7

Now the time of the two storm-time substorm onsets (AL minima) are indicated in Figs 4-6. As far as an expansion during the growth phase, and then a contraction is concerned, the effect is almost not seen for the event under consideration. It is likely because we deal with the equatorward but not the poleward boundary. It is rather the poleward boundary of FACs that is closely related to the polar cap (open-close) boundary displacement in the course of substorm development. However, in the parameter presented here (the equatorward boundary and the current intensity), it is difficult to reveal the effect of expansion/contraction. The following comment has been added to Section 4 *Dynamics of the equatorward boundary* (p. 15, ll. 16-29 - p.16, ll. 1-2).

"Upon arrival of the SW shock at the very end of September 7, EqB is abruptly shifted equatorward, then tends to recover until the middle of September 8, and then drops again following the second intensification of the storm. At the very beginning of 8 September EqB is found at its lowest position at 50° MLat. A drop of EqB occurs simultaneously with the peak of the first storm-time substorm just between 7 and 8 September and with the lowest SYM-H (below -150 nT). The second substorm reaches its peak slightly before the second minimum of SYM-H (at 12:50 and 13:55, respectively). During this second activation the EqB is shifted again as low as 50° MLat (although SYM-H is only -100 nT). As seen in Fig. 5, the evolution of EqB tends to follow the gradual change of SYM-H rather than an abrupt drops of AL related to the substorm onset (see also Fig. 2 for AL). Unlike the nightside current density, which exhibits several spike-like increases in accordance with AL and the dayside density, which is enhanced

throughout the storm, temporal variations of EqB are relatively smooth and tend to follow the SYM-H index. In the end of September 9, during the late recovery phase of the storm, EqB is shifted poleward as high as 70° MLat. As far as the day-night asymmetry is concerned, almost no difference in evolution on the day- and nightside EqBs is observed during the main and recovery phases. Because the storm-time substorms are relatively short-lived, an expansion of the FAC region during the growth phase, and then a contraction are difficult to resolve with the *Swarm* data.”

Comment 1.8

I think the description of dawn/dusk asymmetries is an example of not choosing the right tool for the job. If you want to investigate global dawn/dusk asymmetries, why not use AMPERE, which provides global FAC maps, instead of Swarm which only gives in-situ measurements?

Reply to Comment 1.8

Yes, AMPERE provides global FAC maps which are suitable to study the asymmetry. However, the AMPERE products are not considered here because the present paper concentrates the Swarm data and intends to reveal the storm-time effects solely in these in-situ measurements. Although the picture presented here is not global, the expected asymmetry can be revealed. Joint analysis of the AMPERE and Swarm data in order to reveal an asymmetry and place the Swarm in situ observations in context may be a subject of future work. The appropriate references for the previous AMPERE results are included (p. 25, l. 15-20).

Comment 1.9

In two cases (l. 25, p. 18 and l. 25 p. 19) reference is made to analyses that are not shown. If it is not shown, it should not be included unless it is completely trivial and easy to check for the reader, which does not seem to be the case here.

Reply to Comment 1.9

Following to this comment, in both cases the text referred to the preliminary, not shown analysis has been eliminated.

Referee #2

General comments

In general, the paper presents a case study, interesting new observations, however, in some cases it is not clear whether the presented observation and result is new or just confirmation of previous findings. This should be clarified and emphasized in the discussion section.

The study of the dawn-dusk asymmetry comparing the dusk-side and dawn-side portions of the same orbit (practically in 1D), especially at small scales, is questionable since this approach ignores the 3D distribution of the current system.

Based on the presented figures and tables the calculation of the MLT is very suspicious (see below in the specific comments). Since the MLT information is essential for the whole analysis that may fundamentally affect all the results and conclusions, the paper cannot be accepted before this serious issue is fixed. There are a series of other smaller issues (listed below) that have to be considered before a possible acceptance.

Reply General comments

All sections have been considerably modified in order to better structuring and emphasis of the new findings.

Yes, the dawn-dusk asymmetry can not be resolved in 1D distribution. This issue was also mentioned in the Referee #1 comments. AMPERE product is more relevant to this kind of analysis. However, it does not exclude a possibility to reveal signatures of such asymmetry even in the instantaneous measurements during a severe magnetic storm. The present paper concentrates the Swarm data and intends to reveal the storm-time effects solely in these in-situ measurements. Although the picture is not global, some signatures of the expected asymmetry can be revealed. Joint analysis of the AMPERE and Swarm data can be a subject of future work.

Concerning the MLT problem please see Reply to Comment 2.5

Comment 2.1

p 3 1 1-10 The description of the storm evolution needs some correction and complementation. Give the time of the shock arrival on 6 Sep. The trigger of the first substorm is first identified as the southward turning Bz at 18:30 on 7 Sep, then a few lines later, as the second shock arriving at 22:00. In contrast with your description, SYM-H was not recovered on 8 Sep.

Reply to Comment 2.1

The description of the storm evolution has been modified as follows (p. 7, ll. 15-18 – p.8, ll. 1-8). “Two SW shock events impact the magnetosphere. The arrival of the first shock late on 6 September (23:50 UT) results in a sudden increase in all parameters except the AL index. Since IMF Bz turns northward, this initial disturbance is only weakly geoeffective as a result. At 20:40 UT, 7 September, IMF Bz turns southward that triggers a substorm growth phase and a ring current build up. The second shock arrived at ~23:40 UT on 7 September, with the SW speed up to 800 km/s and strongly negative Bz and By. This shock causes an abrupt drop of SYM-H down to -150 nT and a spike-like decrease of AL down to -2200 nT. After 03 UT, 8 September, the IMF Bz becomes positive, AL gradually approaches to zero and SYM-H starts to recover until the next southward turn of Bz. At ~06 UT on 8 September another strongly negative Bz period is seen, and the SW speed remains high (>700 km/s). This causes the second substorm (AL is -

2000 nT) and ring current intensification (SYM-H is -100 nT). A steady recovery occurs in the AL index throughout 9 September, while the SYM-H gradually increases from -75 to -35 nT. The SW parameters are not available for this day.”

Comment 2.2

p 4 1 4 and 6 Description of the Swarm constellation has to be revised. The orbit inclination for SwB is different from that of the other two. As a consequence, the separation between B and (A and C) is increasing. In Sep 2017 it was already close to 6 h (and not 1.5 h) as you can easily check on your Fig. 2. p 4 1 6 The slow drift is in MLT not in longitude. p4 1 7 Since any orbit consists of two parts separated in local time by 12 h, you only need around 4 and a half (and not 7-10) month of data to cover all local times.

Reply to Comment 2.2

Corrected. In section 2.1 the description of the orbits has been modified as follows (p. 4, ll. 14-19).

“SwA and SwC fly in a tandem separated by 1-1.4° in longitude and the differential delay in orbit is ~3 s. The orbit period is about 93 min and slightly different between SwA/SwC and the upper satellite SwB, so that their along-orbit separation in local time gradually changes. Their orbital planes also gradually drift apart and the separation angle increases by ~20° longitude per year. Slowly drifting in longitude, the orbits cover all the local time sectors over about 130 days.”

Comment 2.3

p 4 1 8 The description of the derivation of the FAC product is very inaccurate (“from the measured magnetic field variations, which results from FACs, the current densities are computed: : :”). You may just describe the Swarm single-satellite FAC product mentioning its limitations.

Reply to Comment 2.3

The description of the derivation of the FAC product has been modified and extended in order to describe the dual- and single-satellite approach. In the revised version the following additional comments have been included to section 2.1 Instrumentation (p. 4, ll. 21-29 – p.5, ll. 1-15).

“The mission has a multi-instrument payload. The main module is the high-sensitivity vector (fluxgate type) and scalar magnetometers for determining the magnitude and direction of the total vector and variations of the geomagnetic field with an accuracy of more than 0.5 nT (Merayo et al., 2008). Magnetometers make it possible to carry out measurements in a wide range, including the Earth’s main magnetic field and the variations of external magnetic field generated by FACs. FACs are detected by their magnetic perturbations in the orthogonal plane which are obtained after subtracting the main magnetic field model from the total measured values. From single spacecraft the FAC density can be estimated based on one magnetic component with a techniques invoking Ampere’s law under assumptions about the infinite current sheet geometry and the orthogonal crossing of the current sheet. This method was used for the previous one-satellite missions, such as Magsat and Ørsted (Christiansen et al., 2002). It is also applied to each *Swarm* satellite separately. The dual-satellite estimation method calculates current density from $\text{curl}(B)$ measured quasi-simultaneously at 4 locations is adapted for SwA and SwC data, where measurements separated along-track are used to create a ‘tetrahedron’ (Ritter and Lühr, 2006). The $\text{curl}(B)$ method provides more reliable current density estimates, as it does not require any assumptions on current geometry and orientation. The FAC output of both a dual-satellite and a single satellite methods are considered to be in a reasonable agreement (Ritter et al., 2013). However, a high degree of coherence is typical at auroral latitudes, while in

the polar cap the results based on dual-spacecraft technique as more reliable (Luhr et al., 2016). Both algorithms are implemented to generate the *Swarm* products that are produced automatically by ESA's processing center as soon as all input data are available. The products are provided using the dual-satellite method on the lower pair of satellites SwA and SwC, and the single-satellite solution for each of the Swarm spacecraft individually. The 1 s values (1 Hz sampling rate) of FAC densities are available via the on-line *Swarm* data portal (<ftp://swarm-diss.eo.esa.int>) as Level 2 data products (Swarm Level 2 Processing System Consortium, 2012). In the present study the single-satellite FACs are used in order to apply the similar method to SwB and SwA/SwC data.”

Comment 2.4

p4 Description of the plasma product is missing.

Reply to Comment 2.4

Added as follows (p. 5, ll.17-22):

“Each satellite is also equipped with the Electric Field Instrument which includes the Langmuir probe to provide measurements of ionospheric plasma parameters: electron density, electron temperature and spacecraft potential (Knudsen et al., 2003). The plasma data are available at 2 Hz sampling rate as the standard product of the *Swarm* data base. Unfortunately, due to technical problems, measurements of the electric field and ions are rather rare. Nevertheless, the combination of data provided by a magnetometer and a plasma analyzer on electrons makes it possible to identify perturbations associated with FACs.”

Comment 2.5

Figure 2 a) From the polar plot presenting the orbits in the MLT-mlat system, it is suspicious that your MLT calculation is not correct. 2 h change in MLT within a few days is not realistic.

Figure 2 b) I cannot make sense of this figure: daily variation of MLT as a function of MLT. On the x-axis, MLT runs from 0-24. And it is not a straight line!

Your MLT calculation has to be revisited and clearly described in the paper.

Table 1 The same MLT issue.

Reply to Comment 2.5

Figure 1 is seemed to be correct. (Note that in the revised version Fig. 1 is Fig. 2 because Section “*Swarm* satellites” and Section “Space weather conditions on 6–9 September 2017” was swapped as recommended by Referee #3. Also, Fig. 2a has been eliminated because the same information on the orbits is presented in Table 1). During the day, the orbits are systematically shifted almost parallel to each other, however, in auroral latitudes, they are within the early in the morning, pre-noon, pre-dawn and pre-midnight sectors. (Projection of *Swarm* satellite passes recalculated to the MLT–MLAT domain during the full day is presented in, e.g., Cherniak and Zakharenkova *Earth, Planets and Space* (2016) 68:136, DOI 10.1186/s40623-016-0506-1; their Fig.1).

Figure 1b (former Figure 2b, eliminated in the revised version) was erroneous. The correct x-axis title is UT.

MLT was not calculated, it was taken from the *Swarm* VirES tool. The following comment has been added (p.5, ll. 23-27):

“In each Level 2 data file the location of the satellite is presented in an geographic coordinate system NEC (x - North, y - East, z - Center), where the x and y components lie in the horizontal plane, pointing northward and eastward, respectively, and z points to the centre of gravity of the

Earth. For the purpose of present study all projections of the passes are shown in the magnetic local time (MLT) and MLat domain. The coordinates are available via the on-line Swarm Data Visualisation Tool (VirES).”

Comment 2.6

Section 4.1 FAC densities You may want to rename this section in relation to the title of Section 4.4 ‘Small-scale FACs’.

Reply to Comment 2.6

I’d prefer to keep the present title because it is more general and actually both the small (1 Hz) and large (averaged) currents are considered.

Comment 2.7

Figure 3 b) and p 6 1 12-13 What I see is R1 upward and R2 downward.

Reply to Comment 2.7

The description of Fig. 3 has been made more precise and modified as follows (p. 9, ll. 19-25): “Fig. 3b depicts the 21-point smoothed curve. It can be seen that the satellite approaching the pole from the dusk observes first the downward (positive) R2 and then the upward (negative) R1 current, both are of $\sim 2 \mu\text{A}/\text{m}^2$ density. Above approximately 70° MLat FACs become marginal. When the satellite moves equatorward in the early morning local times, a multi-layer structure is observed, in which the poleward currents are mostly positive, so they may be associated with downward the R1 FAC. The most equatorward currents are negative and thus represent the R2 FAC.”

Comment 2.8

p 7 1 5-6 This wording (“determined by averaging the positive (negative) FAC densities from a current free location at the lowest and highest MLat of each crossing”) is confusing, rephrase. What is the advantage of using the average densities instead of the ‘total’ (integrated?) densities? As you mention, the two correlates. Does it mean that the variation of the range of FAC latitudes is not significant?

Reply to Comment 2.8

The confusing description has been rephrased. In the revised version it sounds as follows (p.10, ll. 6-9):

“To demonstrate the global temporal evolution of FACs, in Fig. 4 the current intensities for the four MLT sectors are presented separately for the northern (Fig. 4 a, c, e, g) and southern (Fig. 4 b, d, f, h) hemispheres. Each red (blue) point is determined by averaging the downward (upward) current densities when the satellite crosses the region filled with FACs.”

The advantage of using the average densities instead of the ‘total’ (summed) densities is related mainly to the different length of the satellite track within the region filled by FAC. Although the average and total densities closely correlate, the correlation is not perfect. This is because the variation of the range of FAC latitudes affects the average density in lesser degree.

Comment 2.9

p 7 1 9 precession?

Reply to Comment 2.9

The word “precession” has been eliminated. The daily variation of the polar projection of the satellite orbit is described in more detail as follows (p. 6, ll. 7-9):

“During a day, the successive projections are systematically shifted almost parallel to each other, however, in auroral latitudes, they stay mainly within the same sectors.”

Also, Table 1 has been modified: MLT range within which the satellite crosses the boundary of 50° (70°) MLat has been added. Fig. 1b has been eliminated because it duplicates Table 1.

Comment 2.10

p 9 1 7 ‘The largest FACs are observed’ > ‘The corresponding/associated FACs are the largest: : :’ (after all the shocks and substorms already mentioned the reader is getting lost)

Reply to Comment 2.10

The description of Fig. 4 has been considerably modified for easier comparison and explanation of the storm/substorm development and FAC evolution. AL and SYM-H indices have been added to the figure. In the revised version the description of Fig. 4 does not contain a confused phrase mentioned in the comment.

Comment 2.11

p 9 1 15 ‘there is no’ > ‘we could not find any’

Reply to Comment 2.11

Corrected

Comment 2.12

p 10 1 10 The definition of the EqB is not clear: “at least eight values before and after the central point do not exceed 0.1 $\mu\text{A}/\text{m}^2$ ” Do you mean the smoothed values? Before and after? Central point of what? Estimate the scale of the considered FACs.

Reply to Comment 2.12

I agree that the description of the procedure of EqB determination was confusing. This was likely because in the previous version the sliding window moved along the track in accordance with the actual satellite track, i.e., entering or leaving the FAC region. In the first case 1-second values “after” the central point of the sliding window should be close to zero. In the second case, values “before” the central point should be close to zero.

In the revised version more simple procedure has been applied. The description has been modified accordingly (p. 14, ll. 14-18):

“The EqB is determined as the lowest MLat at which FACs are terminated. The procedure of the 20-point sliding window (the scale is about 150 km) moving along a track from the equator to the pole is applied to the 1 s FAC values and the corresponding MLats. EqB is selected as the lowest MLat of the window if 90% of FAC values within the window exceed $|0.1| \mu\text{A}/\text{m}^2$.”

Comment 2.13

p 10 1 19 “considerable” > “moderate”

p 11 1 8 “is seen only : : : unaffected” > “is the largest : : : less affected”

Reply to Comment 2.13

Corrected

Comment 2.14

Figure 5 MLT values given in the figure caption and in the legend are different

Reply to Comment 2.14

Corrected

Comment 2.15

p 12 1 6 “resolved spatial scale” > “spatial resolution”

p 13 1 5 and 7 Reference to Fig 7a and 7b are exchanged

Reply to Comment 2.15

Corrected

Comment 2.16

p 14 1 10 FFT?? Isn’t it just a boxcar smoothing?

Reply to Comment 2.16

A boxcar (build-in to the Matlab/Origin) FFT procedure is used. “FFT” is removed from the text.

Comment 2.17

p 14 1 17 20000-40000 cm-3 seems a bit low for topside Ne, please confirm

Reply to Comment 2.17

These values are what is available via the Swarm data portal

Comment 2.18

p 14 1 19 Note, that as far as I know, the Swarm Te values are still uncalibrated. If still so, please make a note.

Reply to Comment 2.18

The data were downloaded from the Swarm data portal. There is no clear indication that they are still uncalibrated. Even if so, it is hardly affect the relatively small-scale perturbations.

Comment 2.19

p 15 1 13 “: : : a decrease in Ne (which is usually much less pronounced than a decrease : : :” ?

p 15 1 14 “are created” > “may be created”

p 17 1 24 “is associated” > “is likely associated”

Reply to Comment 2.19

Corrected

Comment 2.20

p 18 1 5 “It confirms the fact” If it is a fact, why does it need confirmation? Your statement that large-scale FACs are composed of more intense small-scale FACs is not supported by your analysis. You also mention that others found that small-scale FACs are mostly associated with Alfvén-waves.

Reply to Comment 2.20

These sentences have been refrased as follows: "This implies that a substantial fraction of R1/R2 currents is composed of many small-scale FACs." (p. 26, ll. 4-5).

Comment 2.21

p 18 l 15 The scale length range in the brackets is for small-scales?. What scale was taken as a large scale? The given density value (0.5) is for large scale? Please clarify.

Reply to Comment 2.21

Corrected (p.26, ll. 16-17). In the cited paper the large scale implies >250 km length and the density value (0.5) is for the small scale.

Comment 2.22

p 19 l 3 Is your definition of EqB of large-scale FACs is comparable to that of the cited paper?

Reply to Comment 2.22

Wang et al. (2006) defined the latitudinal positions of peak current density but not the most equatorward boundary of the FAC region, thus the actual FAC region may expand to lower latitudes (below the reported 52-56° MLat). A note has been made (p. 24, ll. 4-6).

Other comments and Technical corrections

p 19 l 15 Image > IMAGE (the name is an acronym)

p 19 l 22 equatorial > equatorward

p 20 l 9 'indication' this asymmetry is well-known, you may say, your observation is in accordance with this.

p 6 l 11 Aan > An

p 7 l 4 is > are

p 9 l 5 and 7 (also elsewhere) 'in the northern hemisphere', 'in the night side', 'in the day side' > 'on the night side', 'on the dayside', 'on the northern hemisphere'

p 9 l 13 'coherence' > 'correlation'

p 14 l 7 (and elsewhere) 1-sec FAC > 1 s FAC or 1 Hz FAC

p 14 l 21 0.4 and 2% > 0.4% and 2%

Reply

Corrected

Referee #3

Comment 3.1

- The first paragraph is written in a bit loose way, e.g. Are FACs flowing only from boundary layers? Why FAC system is evolved only by dayside (not nightside) reconnection? FAC may exceed its nominal level – what is meant by nominal level?

Reply to Comment 3.1

The first para of Introduction has been rewritten in order to address the issues pointed out by Referee. The revised version reads as follows (p. 1, ll. 27-34 – p. 2, ll. 1-17).

“Field-aligned currents (FACs) provide electrodynamic coupling of the solar wind-magnetosphere-ionosphere system. FACs flow along the high-conducting geomagnetic field lines between different magnetospheric domains and the high latitude ionosphere. This current system is driven by the internal magnetospheric circulation of plasma and magnetic field within the global reconnection cycle (Dungey, 1961) and by additional viscous-like interaction at the flanks of magnetosphere (Axford, 1964). Configuration of FACs is primarily controlled by the interplanetary magnetic field (IMF) orientation. Other parameters of the solar wind (velocity, density, IMF strength) and the ionospheric conductivity also play a role (e.g. Christiansen et al., 2002; Ridley 2007; Korth et al., 2002).

Schematic distribution of large-scale FACs has been established by Iijima and Potemra (1976) based on the Triad satellite data. Subsequent space missions allowed constructing comprehensive empirical models of FAC parameterized by the IMF direction and strength, by season, and by hemisphere (Weimer, 2001; Papitashvili et al., 2002; Green et al., 2009). The ionospheric projection of the 3D FAC system consists of a pair of sheets elongated along the auroral oval, namely, Region 1 (R1) and Region 2 (R2), with opposite current flow directions in the morning and evening local time sectors and additional current sheets (R0) located on the dayside poleward of R1/R2. R1 flows into the ionosphere (downward current) and from the ionosphere (upward current) on the dawn and dusk side, respectively. R1 currents, if reside on closed field lines of the Earth’s magnetic field, are believed to originate in either the boundary layer or in the plasma sheet (Ganushkina et al., 2015). R2 FAC is considered to be a diversion of the partial ring current to the ionosphere driven by pressure gradients in the inner magnetosphere (Cowley, 2000). R0 current is connected to the dayside magnetopause and its polarity strongly depends on the IMF B_y component. On the Northern Hemisphere, the R0 current flows predominantly out of the ionosphere for positive IMF B_y and into the ionosphere for negative IMF B_y (Papitashvili et al., 2002; Lukianova et al., 2012). Additional (NBZ) current associated with the sunward ionospheric flow may appear inside the polar cap, if IMF B_z is northward (Iijima et al., 1984; Vernerstrøm et al., 2002).

Comment 3.2

In the second paragraph it is said that Wang et al. (2006) and Anderson and Korth (2008) have studied storms, but no results are given.

Reply to Comment 3.2

A brief description of the results obtained by the authors cited has been added to the 5th para (former 2nd) as follows (p. 3, ll. 16-28).

“Utilizing the magnetic field measurements by CHAMP satellite Wang et al. (2006) investigated the northern and southern hemisphere dayside and nightside FAC characteristics during the

extreme October and November 2003 magnetic storms. It was shown that as Dst decreases, the FAC region expand equatorward, with the shift of FACs on the dayside controlled by the southward IMF. For both case studies, on the southern (late spring) hemisphere the minimum latitude of the FACs is limited to 50° magnetic latitude (MLat) for large negative values of Bz (The minima are the same, although in October the IMF Bz drops down to -28 nT, while in November it reaches -50 nT.) On the northern (late autumn) hemisphere the equatorward boundaries of the FAC region are located at 55-60° MLat. Using the global maps from the Iridium constellation Anderson et al. (2005) studied the FACs intensities during severe magnetic storms which occurred during the solar cycle 23 with a particular attention to the evolution of FACs in the course of the storm of August 2000. The results revealed the dawn-dusk asymmetry of the R1/R2 current sheets, with an increase primarily found on the duskside. It was shown that under disturbed conditions the total current is not linearly related to the interplanetary electric field, with the intensity constrained to be below 20 MA (Anderson and Korth, 2007)."

Comment 3.3

Please swap Sections 2 and 3, it would be more logical.

Reply to Comment 3.3

Done. Also, Section 2 *Swarm satellites* has been divided into two subsections: 2.1 *Instrumentation* (descriptions of the methods used for FAC derivation and the EFI instrument have been added) and 2.2 *Orbits on 6-9 September 2017*.

Comment 3.4

Section 2:

- Maybe the Clilverd et al. (2008) paper should be referred to?

Reply to Comment 3.4

Unfortunately I did not understand what paper by Clilverd et al. (2008) the Referee advises. In the 1st para of Section 3 Space weather conditions on 6–9 September 2017 (former Section 2) I refer to several recent papers, including Clilverd et al., 2018, in which the different effects of the September 2017 storm were analyzed.

Comment 3.5

Section 3:

- Here one should shortly explain how 1-s FAC data products are derived from the original magnetometer data

Reply to Comment 3.5

The description of FAC data products has been added to Section 2.1 *Instrumentation* (former Section 3) as follows (p. 4, ll. 21-29 – p. 5, ll. 1-15).

“The mission has a multi-instrument payload. The main module is the high-sensitivity vector (fluxgate type) and scalar magnetometers for determining the magnitude and direction of the total vector and variations of the geomagnetic field with an accuracy of more than 0.5 nT (Merayo et al., 2008). Magnetometers make it possible to carry out measurements in a wide range, including the Earth’s main magnetic field and the variations of external magnetic field generated by FACs. FACs are detected by their magnetic perturbations in the orthogonal plane which are obtained after subtracting the main magnetic field model from the total measured values. From single spacecraft the FAC density can be estimated based on one magnetic component with a techniques

invoking Ampere's law under assumptions about the infinite current sheet geometry and the orthogonal crossing of the current sheet. This method was used for the previous one-satellite missions, such as Magsat and Ørsted (Christiansen et al., 2002). It is also applied to each *Swarm* satellite separately. The dual-satellite estimation method calculates current density from $\text{curl}(B)$ measured quasi-simultaneously at 4 locations is adapted for SwA and SwC data, where measurements separated along-track are used to create a 'tetrahedron' (Ritter and Lühr, 2006). The $\text{curl}(B)$ method provides more reliable current density estimates, as it does not require any assumptions on current geometry and orientation. The FAC output of both a dual-satellite and a single satellite methods are considered to be in a reasonable agreement (Ritter et al., 2013). However, a high degree of coherence is typical at auroral latitudes, while in the polar cap the results based on dual-spacecraft technique are more reliable (Lühr et al., 2016). Both algorithms are implemented to generate the *Swarm* products that are produced automatically by ESA's processing center as soon as all input data are available. The products are provided using the dual-satellite method on the lower pair of satellites SwA and SwC, and the single-satellite solution for each of the Swarm spacecraft individually. The 1 s values (1 Hz sampling rate) of FAC densities are available via the on-line *Swarm* data portal (<ftp://swarm-diss.eo.esa.int>) as Level 2 data products (Swarm Level 2 Processing System Consortium, 2012). In the present study the single-satellite FACs are used in order to apply the similar method to SwB and SwA/SwC data."

Comment 3.6

- Please explain what coordinate system for MLAT is used and how MLAT and MLT are derived

Reply to Comment 3.6

The following explanation on the coordinate system has been added (p. 5, ll. 22-27).

"In each Level 2 data file the location of the satellite is presented in an geographic coordinate system NEC (x - North, y - East, z - Center), where the x and y components lie in the horizontal plane, pointing northward and eastward, respectively, and z points to the centre of gravity of the Earth. For the purpose of present study all projections of the passes are shown in the magnetic local time (MLT) and magnetic latitude (MLat) domain. For this the coordinates are available via the on-line Swarm Data Visualisation Tool (VirES)."

Comment 3.7

- SwB is not separated by 1.5 h in LT from SwA and C, but this difference depends on time

Reply to Comment 3.7

This erroneous statement has been corrected. Now the corresponding para in Section 2.1 *Instrumentation* reads as follows (p. 4, ll. 14-19).

"SwA and SwC fly in a tandem separated by 1-1.4° in longitude and the differential delay in orbit is ~3 s. The orbit period is about 93 min and slightly different between SwA/SwC and the upper satellite SwB, so that their along-orbit separation in local time gradually changes. Their orbital planes also gradually drift apart and the separation angle increases by ~20° longitude per year. Slowly drifting in longitude, the orbits cover all the local time sectors over about 130 days."

Comment 3.8

- First sentence in Sect. 4.1.: give a reference

Reply to Comment 3.8

The references to (Weimer, 2001; Papitashvili et al., 2002; Green et al., 2009) have been added.

Comment 3.9

- Figure 3: Define FAC positive values (up- or downward current)

Reply to Comment 3.9

Definition has been added to the figure caption: “Downward (upward) current is positive (negative)”.

Comment 3.10

Figure 4: It would be more informative for the reader to see in the upper right corner the mean MLT value (or text “pre-noon” etc) than the track identifier. One could also add standard deviations to the mean values by error bars (and expand the horizontal width of the figure)

Reply to Comment 3.10

Figure 4 has been re-plotted. Standard deviations, the centered MLT (instead of the track identifier) and SYM-H and AL indices have been added. Shading has been eliminated to avoid a overloading of the figure. The description of the figure has been modified accordingly. The revised version reads as follows (p. 10, ll. 6-16 - p. 12, ll. 1-15).

“To demonstrate the global temporal evolution of FACs, in Fig. 4 the current intensities for the four MLT sectors are presented separately for the northern (Fig. 4 a, c, e, g) and southern (Fig. 4 b, d, f, h) hemispheres. Each red (blue) point is determined by averaging the downward (upward) current densities when the satellite crosses the region filled with FACs. The upper (a - d) and lower (e - h) plots represent the data from the day side (10 and 16 MLT) and night side (04 and 22 MLT), respectively. For easier visual association of the evolution of FACs with the storm development, the SYM-H and AL indices are added in the plots (a, b) representing the day side and in the plots (e, f) representing the night side, respectively. During 6-9 September, FACs shown in Fig. 4, exhibit three pronounced enhancements, which are of different intensity depending on the MLT sectors. (Note that the FAC densities do not show any systematic changes associated with the orbit oscillation during the day.) All FACs start to increase in the very beginning of September 7 in association with the SW dynamic pressure front impinges the magnetosphere causing a positive excursion of SYM-H. The dayside FACs increase abruptly (this is especially well seen in Fig. 4 b - c, i.e. at 10 MLT, north, and at 16 MLT, south), while the nightside FACs (Fig. 4 e - h) respond to the shock with a considerable delay. The nightside FACs are peaked in the middle of September 7, when a moderate substorm occurs.

In the very beginning of September 8, in association with the first deep drops of SYM-H and AL, a step-like increase is seen at all MLTs except the prenoon sector. The peak of the day- and nightside FACs reaches 2.5 and $3.5 \mu\text{A}/\text{m}^2$, respectively. For a particular crossing the average density exceeds $5-6 \mu\text{A}/\text{m}^2$ as seen from the standard deviation. The dayside FACs (Fig. 4 a - d) stay enhanced during the whole day of 8 September. The nightside FACs (Fig. 4 e - h) more closely follow the evolution of AL, so that the current intensities decrease in accordance with the first storm-time substorm recovery. The next increase in the nightside FACs occurs at ~ 12 UT on September 8, when the second major substorm occurs and the second drop in SYM-H is observed. On the day side the response of FACs to this substorm is marginal, although the current densities remain elevated throughout the day. All FACs fall to pre-storm levels by September 9.”

Comment 3.11

Table 2 would need more explanation. Which MLATs are included in the calculation? What are the uncertainty limits behind these numbers? Has the author checked from the Southern hemisphere, which are the highest MLATs that the satellites reach and does that affect the estimates?

Reply to Comment 3.11

MLAT for 50° – 90° is accounted. It is difficult to estimate the uncertainty behind the numbers presented in Table 2. The number itself has no uncertainty because this is a result of the straightforward summation. At the same time, as pointed out by the Referee, there may be indirect factors which lead to under- or overestimation of the currents. In this connection the following additional explanation for Table 2 has been included (p. 13, ll. 23-26).

“Although the numbers in Table 2 contain uncertainties related to the lack of global observations, the estimate based on the summed FAC densities from in-situ *Swarm* measurements indicate the existence of the storm-time dawn-dusk asymmetry. Even a limited number of crossings show a clear tendency of the prevalence of the dusk-side R2.”

Comment 3.12

- Line 29: “From the FAC values presented in columns 5 and 6 one can see that in both hemispheres the dusk side downward current is stronger than all the other currents. This predominance implies an additional amplification of the storm-time R2 FAC on the dusk side, which is related to the partial ring current.” This would need more discussion and definitely a reference.

Reply to Comment 3.12

The following addition has been made (p. 13, ll. 27-29).

“This shift may result from a strong dusk side ion pressure leading to asymmetric dusk-side inflation of the magnetic field consistent with a partial, dusk side, ring current during storm main phase (Liemohn et al., 2001; Anderson and Korth, 2007).”

Comment 3.13

- “pre-storm time”. It would be good to define from the beginning, what is the onset of the storm time, and maybe mark that in all the figures.

Reply to Comment 3.13

The pre-storm time is defined as the time before the SYM-H attains its stable negative values <20 nT at 22:00 on 7 September. In the revised version, for easier comparison of the FAC evolution with the storm phases the AL and SYM-H indices are added to Fig. 4, SYM-H is added to Fig. 5. In Figs 5 and 6 the time when the SYM-H attains its stable negative values <20 nT at 22:00 on 7 September and the time of AL minima are marked by vertical lines.

Comment 3.14

- 1. 18 “Comparing Fig. 1 and Fig. 4 one can see that EqB more closely follows the variation of SYM-H.” I agree that since end of Sept 7, the boundaries seem to follow SYM-H, but not before that. Maybe the author could check the correlation to AE-index as well?

Reply to Comment 3.14

I do not think that the correlation between AE and EqB would help to resolve the dependence of EqB on any single parameter. For easier comparison the SYM-H index has been added to Fig. 5. More explanation on the SYM-H and EqB coherence has been added to Section 4.3 as the follows (p. 15, ll. 1-14).

“Even visual comparison of the SYM-H and EqB evolutions in Fig. 5 reveals generally coherent behavior of these two parameters. In particular, during a period preceding the storm main phase (before 8 September, when SYM-H is mainly positive) EqB is located much lower than during the end of recovery phase (after ~12 UT on 9 September, when SYM-H is still negative). Before the SYM-H attains its stable negative values <-20 nT at 22:00 on 7 September FACs are observed mainly poleward of 60° MLat on both hemispheres. Moderate equatorward shifts of EqB are associated with the modest substorms occurred before the storm main phase in the middle of 6 and 7 September. Prior the main phase, on both hemispheres the prenoon (04 MLT) EqB is found considerably poleward compared to the EqB location at other MLTs. The effect is well seen during the two time intervals: from ~22 UT, September 6 till 06 UT, September 7 and at 12-24 UT, September 7. Both intervals are dominated by the northward IMF (sf. Fig. 2), so that a shrinking of the polar cap and a poleward shift of the auroral oval is expected. With regard to the position of FACs, the displacement of its equatorward boundary is the largest only in the pre-noon sector, while the other local times remain less affected.”

Comment 3.15

“The current intensity vary inversely with scale”. Please give a reference.

Reply to Comment 3.15

The references to (Neubert and Christiansen, 2003; McGranaghan et al., 2017) have been added.

Comment 3.16

It is unclear how Figure 7 is composed. What are the horizontal and vertical axes? Is the figure even needed in this paper?

Reply to Comment 3.16

Fig. 7 seems curious because it demonstrates the bipolar structure (closely adjacent small-scale FACs of opposite polarity) occurrence in different MLTs. On the day- and night side they are likely associated with the reconnection formed at the magnetopause and mesoscale auroral arcs, respectively. To make it more clear how the figure is composed the title of x and y axis has been modified as MLat “down” and MLat “up”, respectively.

The following explanation for Fig. 7 has been added to Section 4.4 (p. 18, ll. 7-17 – p. 19, ll. 1-3) and 5.2 (p. 27, ll. 15-28).

“When for each crossing within a certain MLT sector, the minimum (i.e. peak upward current) and the maximum (i.e. peak downward current) 1 s FACs are selected, it appears that in some cases these peaks are observed at very close latitudes, while in other cases the minimum and maximum are spaced in latitude. In Fig. 7, the correlations between the MLats, at which the most intense small-scale FACs of opposite polarities are observed, are presented for each MLT sectors. The x-axis (y-axis) corresponds to the MLat of the downward (upward) peak selected in each crossing. The magnitude of minima and maxima are not accounted. From Fig. 7 one can see that correlation between the latitudinal positions of the up- and downward peaks varies with MLT. The highest correlation coefficient ($cc=0.94$) is found in the pre-noon sector (Fig. 7b).

This is indicative of a large population of the paired, closely adjacent small-scale currents of opposite polarity (called hereafter the bipolar structure). In the dusk (Fig. 7a) the correlation coefficient decreases down to 0.78. Almost the same correlation ($cc=0.75$) is observed in the pre-midnight sector (Fig. 7c). At the early morning hours (Fig. 7d) the correlation is much weaker ($cc=0.53$) implying that the extreme up- and downward currents appear less frequently in pair but rather are spatially (or temporary) separated. Different mechanisms of the small-scale FAC formation on the day- and night side can be the cause of this spatial distribution and variability.”

“Statistically, the bipolar structures dominate in the pre-noon. In the post-midnight MLTs they are observed less frequently. While the interpretation of the bipolar structure in the terms of the meso-scale arc pattern seems reasonable, the small-scale FACs are often a result of reconnection processes distributed over the dayside magnetopause and even in the tail for negative B_z . In contrast to the post-midnight, in the pre-noon sector, where cusp/cleft currents are expected, the bipolar structures are quite frequent. This may be a signature of the plasma injections which are accompanied by pairs of FACs generated due to flux transfer event (FTE) formation (Southwood, 1987) or multiple reconnection at the magnetopause. Magnetic topologies associated with FTEs were previously observed by the MEO satellites (Marchaudon et al., 2004; 2006; Pu et al., 2013). The small-scale field-aligned currents are possibly a consequence of turbulence and instabilities associated with the process of opening previously closed magnetospheric field lines and merging them with the interplanetary magnetic field (Watermann et al., 2009). The regularity presented in **Fig. 7** shows that during the September 2017 magnetic storm the bipolar structures dominate exactly in the region where the signatures of FTEs and the reconnection lines formed at the magnetopause are expected. At the same time, a pair of the most intense FACs is observed on the night side.”

Comment 3.17

- In this section suddenly Te and U_{sc} are discussed without anywhere properly explained, how it has been derived (which instrument, references etc)

Reply to Comment 3.17

A brief description of the plasma instrument has been added to Section 2.1 *Instrumentation* (p. 5, ll. 17-22).

Comment 3.18

- “The considerably elevated Te within the arc and just poleward of the arc is associated with a local amplification of electric field.” I don’t understand this sentence. To my understanding, electric field data is not used in this study. Furthermore, why Te enhancement would be associated with enhanced EF?

Reply to Comment 3.18

Yes, the electric field data is not used in this study because the Swarm electric field is unavailable. Thus I can only referee to previous observations, e.g. by Aikio et al. (2002) and Kozlovsky et al. (2007). And indeed, it is not necessary the Te enhancement would be associated with enhanced EF.

Comment 3.19

Reference to Wang et al. (2004) is not found from the list. maybe it should be 2006?

Reply to Comment 3.19

Wang et al. (2006) is correct.

Swarm field-aligned currents during a severe magnetic storm of September 2017

Renata Lukianova^{1,2}

¹ Space Research Institute, 117997 Moscow, Russia

² Institute of Earth Science, Saint Petersburg State University, 199034 Saint Petersburg, Russia

Correspondence to: Renata Lukianova (renata@aari.nw.ru)

Abstract. *Swarm* satellites observations are used to characterize the extreme behavior of large- and small-scale field-aligned currents (FACs) during the severe magnetic storm of September 2017. Evolution of the current intensities and the equatorward displacement of FACs are analyzed while the satellites cross the pre-midnight, pre-noon, dusk and dawn sectors on both hemispheres. The equatorward boundaries of FACs mainly follow the dynamics of ring current as monitored in terms of the SYM-H index. The minimum latitude of the FAC boundaries is limited to 50° MLat. The FAC densities are very variable and may increase dramatically, especially on the nightside ionosphere during the storm-time substorms. At the peak of substorm, the average FAC densities reach $>3 \mu\text{A/m}^2$. The dawn-dusk asymmetry is manifested in the enhanced dusk-side R2 FACs on both hemispheres. In the 1 Hz data filamentary high-density structures are always observed confirming that a substantial fraction of R1/R2 FACs is composed of many small-scale currents. In the pre-noon sector, the bipolar structures (7.5 km width FACs of opposite polarities adjacent to each other) dominate, while at the other local times the upward and downward FACs tend to be latitudinally separated. The most intense small-scale FACs, up to $\sim 80 \mu\text{A/m}^2$, is observed just in the post-midnight sector. Simultaneous magnetic and plasma perturbations indicate that this structure is likely a current system of a mesoscale auroral arc.

Keywords: Ionosphere-magnetosphere interaction, Field-aligned currents, Storms and substorms, Auroral arcs electrodynamics

25

1 Introduction

Field-aligned currents (FACs) provide electrodynamic coupling of the solar wind-magnetosphere-ionosphere system. FACs flow along the high-conducting geomagnetic field lines between different magnetospheric domains and the high latitude ionosphere. This current system is driven by the internal magnetospheric circulation of plasma and magnetic field within the global reconnection cycle (Dungey, 1961) and by additional viscous-like interaction at the flanks of magnetosphere (Axford, 1964). Configuration of FACs is primarily controlled by the interplanetary magnetic field (IMF) orientation. Other parameters of the solar wind (velocity, density, IMF strength) and the ionospheric conductivity also play a role (e.g. Christiansen et al., 2002; Ridley 2007; Korth et al., 2002).

Schematic distribution of large-scale FACs has been established by Iijima and Potemra (1976) **based on the Triad satellite data**. Subsequent space missions allowed constructing comprehensive empirical models of FAC parameterized by the IMF direction and strength, by season, and by hemisphere (Weimer, 2001; 5 Papitashvili et al., 2002; Green et al., 2009). The ionospheric projection of the 3D FAC system consists of a pair of sheets elongated along the auroral oval, namely, Region 1 (R1) and Region 2 (R2), with opposite current flow directions in the morning and evening local time sectors and additional current sheets (R0) located on the dayside poleward of R1/R2. R1 flows into the ionosphere (downward current) and from the ionosphere (upward current) on the dawn and dusk side, respectively. R1 currents, if reside on closed field 10 lines of the Earth's magnetic field, are believed to originate in either the boundary layer or in the plasma sheet (Ganushkina et al., 2015). R2 FAC is considered to be a diversion of the partial ring current to the ionosphere driven by pressure gradients in the inner magnetosphere (Cowley, 2000). R0 current is connected to the dayside magnetopause and its polarity strongly depends on the IMF By component. On the Northern Hemisphere, the R0 current flows predominantly out of the ionosphere for positive IMF By 15 and into the ionosphere for negative IMF By (Papitashvili et al., 2002; Lukianova et al., 2012). Additional (NBZ) current associated with the sunward ionospheric flow may appear inside the polar cap, if IMF Bz is northward (Iijima et al., 1984; Vennerstrøm et al., 2002).

While average **large-scale** current densities typically are of units of $\mu\text{A}/\text{m}^2$ or less, instantaneous small- 20 scale FACs may reach several hundred $\mu\text{A}/\text{m}^2$ (Neubert and Christiansen, 2003). The smaller-scale structures are often associated with auroral arcs which are accompanied by ionospheric conductivity and electric field perturbations (Aikio et al., 2002; Juusola et al., 2016). In particular, it was shown that in the evening (morning) sector, there is downward FAC equatorward (poleward) of the arc and upward FAC above the arc. These two FAC regions are connected by a poleward (equatorward) horizontal current. 25 Recent studies also confirmed that the cusp plasma injections are accompanied by pairs of FACs, upward at lower latitude and downward at higher latitude (Marchaudon et al., 2006).

Significant differences in the characteristics of FACs at different scales, especially near noon and midnight have been found (Gjerloev et al., 2011; Luhr et al., 2015; McGranaghan et al., 2017). Under stationary 30 conditions the FAC system is evolved in accordance with the **reconnection rate**, which is controlled

primarily by the solar wind. If a substorm occurs, additional FACs form a current wedge connecting the cross-tail current and the nightside westward ionospheric electrojet (Akasofu, 1964; Lui 1996). The magnitude of existing large-scale FACs also increases (Iijima and Potemra, 1978; Coxon et al., 2014). The dayside R1 currents are found to be stronger than their nightside counterpart during the substorm growth phase, at the same time the R1 oval location moves equatorward. After expansion phase onset, the nightside R1 currents dominate and R1 location moves to higher latitudes (Clausen et al. (2013)). Recent studies have also suggested that the substorm current wedge could also include a R2 current system (Ritter and Lühr, 2008).

10 Magnetic storms are characterized by a dramatic enhancement of energy deposition to the Earth's atmosphere. During a magnetic storm, FACs become highly dynamic because of the enhanced solar-wind-magnetosphere interaction, release of energy stored previously in the magnetotail, particle precipitation and ring current build up. Storm-time FACs are stronger and more variable compared to stationary FACs predicted by the climatological models and the extreme values are often reached. Since the intensity and time evolution of FACs vary

15 from storm to storm, it is of interest to analyze their unique characteristics. However, relatively few papers focus on observed storm-time FACs. Utilizing the magnetic field measurements by *CHAMP* satellite Wang et al. (2006) investigated the northern and southern hemisphere dayside and nightside FAC characteristics during the extreme October and November 2003 magnetic storms. It was shown that as Dst decreases, the FAC region expand equatorward, with the shift of FACs on the dayside controlled by the southward IMF. For both case studies, on the

20 southern (late spring) hemisphere the minimum latitude of the FACs is limited to 50° magnetic latitude (MLat) for large negative values of Bz (The minima are the same, although in October the IMF Bz drops down to -28 nT, while in November it reaches -50 nT.) On the northern (late autumn) hemisphere the equatorward boundaries of the FAC region are located at 55-60° MLat. Using the global maps from the *Iridium* constellation Anderson et al. (2005) studied the FACs intensities during severe magnetic storms which occurred during the solar cycle 23 with a particular

25 attention to the evolution of FACs in the course of the storm of August 2000. The results revealed the dawn-dusk asymmetry of the R1/R2 current sheets, with an increase primarily found on the duskside. It was also shown that under disturbed conditions the total current is not linearly related to the interplanetary electric field, with the intensity constrained to be below 20 MA (Anderson and Korth, 2007).

30 Since 2014, comprehensive studies of FAC distributions were carried out based on high precision observations onboard of *Swarm* constellation (e.g. Dunlop et al., 2015; Juusola et al., 2016; McGranaghan et al., 2017). However, the *Swarm* data have not yet been fully utilized for the storm-time FAC analysis. It is the purpose of this paper to

characterize the magnitude and position of the large- and smaller scale FACs as their response to the magnetic storm development. The *Swarm* observations are used in order to identify various characteristics of the storm-time FACs for the event of 6–9 September 2017, which was one of the two most severe magnetic storms of the recent solar cycle 24 (the previous event was the St-Patrick storm on 17 March 2015). The September 2017 event is of 5 particular interest because it was a two-step storm during which two major substorms occurred and the FAC system is affected by the storm-substorm interplay. In this paper we investigate the time evolution of the large scale FAC intensities, the displacement of the FAC equatorward boundaries and the extreme small scale currents.

2 *Swarm* satellites

2.1 Instrumentation

10 The ESA *Swarm* mission is a constellation consisting of the three identical satellites (hereafter SwA, SwB and SwC, respectively), all are at the low-altitude polar orbit (Friis-Christensen et al., 2008). The *Swarm* constellation was launched in the end of 2013 and entered the operational phase in April 2014. The initial orbit altitude is 465 km (SwA and SwC) and ~520 km (SwB) and the inclination is 87.5°. By September 2017 the orbit altitude decreases down to ~440 and 505 km, respectively. SwA and SwC fly in a tandem 15 separated by 1–1.4° in longitude and the differential delay in orbit is ~3 s. The orbit period is about 93 min and slightly different between SwA/SwC and the upper satellite SwB, so that their along-orbit separation in local time gradually changes. Their orbital planes also gradually drift apart and the separation angle increases by ~20° longitude per year. Slowly drifting in longitude, the orbits cover all the local time sectors over about 130 days.

20 The mission has a multi-instrument payload. The main module is the high-sensitivity vector (fluxgate type) and scalar magnetometers for determining the magnitude and direction of the total vector and variations of the geomagnetic field with an accuracy of more than 0.5 nT (Merayo et al., 2008). Magnetometers make it possible to carry out measurements in a wide range, including the Earth's main magnetic field and the 25 variations of external magnetic field generated by FACs. FACs are detected by their magnetic perturbations in the orthogonal plane which are obtained after subtracting the main magnetic field model from the total measured values. From single spacecraft the FAC density can be estimated based on one magnetic component with a techniques invoking Ampere's law under assumptions about the infinite current sheet geometry and the orthogonal crossing of the current sheet. This method was used for the previous one-

satellite missions, such as Magsat and Ørsted (Christiansen et al., 2002). It is also applied to each *Swarm* satellite separately. The dual-satellite estimation method calculates current density from $\text{curl}(B)$ measured quasi-simultaneously at 4 locations is adapted for SwA and SwC data, where measurements separated along-track are used to create a ‘tetrahedron’ (Ritter and Lühr, 2006). The $\text{curl}(B)$ method provides more reliable current density estimates, as it does not require any assumptions on current geometry and orientation. The FAC output of both a dual-satellite and a single satellite methods are considered to be in a reasonable agreement (Ritter et al., 2013). However, a high degree of coherence is typical at auroral latitudes, while in the polar cap the results based on dual-spacecraft technique are more reliable (Luhr et al., 2016). Both algorithms are implemented to generate the *Swarm* products that are produced automatically by ESA’s processing center as soon as all input data are available. The products are provided using the dual-satellite method on the lower pair of satellites SwA and SwC, and the single-satellite solution for each of the *Swarm* spacecraft individually. The 1 s values (1 Hz sampling rate) of FAC densities are available via the on-line *Swarm* data portal (<ftp://swarm-diss.eo.esa.int>) as Level 2 data products (Swarm Level 2 Processing System Consortium, 2012). In the present study the single-satellite FACs are used in order to apply the similar method to SwB and SwA/SwC data.

Each satellite is also equipped with the Electric Field Instrument which includes the Langmuir probe to provide measurements of ionospheric plasma parameters: electron density, electron temperature and spacecraft potential (Knudsen et al., 2003). The plasma data are available at 2 Hz sampling rate as the standard product of the *Swarm* data base. Unfortunately, due to technical problems, measurements of the electric field and ions are rather rare. Nevertheless, the combination of data provided by a magnetometer and a plasma analyzer on electrons makes it possible to identify perturbations associated with FACs. In each Level 2 data file the location of the satellite is presented in an geographic coordinate system NEC (x - North, y - East, z - Center), where the x and y components lie in the horizontal plane, pointing northward and eastward, respectively, and z points to the centre of gravity of the Earth. For the purpose of present study all projections of the passes are shown in the magnetic local time (MLT) and magnetic latitude (MLat) domain. For this the coordinates are available via the on-line Swarm Data Visualisation Tool (VirES).

.

2.2 Orbits on 6-9 September 2017

The polar projection of the satellite orbits (14-15 trajectories per day) as of September 6-9, 2017 on the northern hemisphere is shown in **Fig. 1a**. For mid-September 2017 the passes are centered in the pre-midnight, pre-noon, pre-dusk and pre-dawn sectors. The satellite SwA (orbits of SwC are very similar) 5 enters the region of MLat $>50^\circ$ between ~ 09 and 12 MLT, and leave this region between ~ 21 and 23 MLT. The entry (exit) points of the SwB orbit are between ~ 15 and 17 (02 and 04) MLT. On the southern hemisphere the direction of the tracks in the MLT-MLat framework is opposite. **During a day, the successive projections are systematically shifted almost parallel to each other, however, in auroral latitudes, they stay mainly within the same sectors.** The MLT ranges covered by the tracks are presented in **Table 1**.

10

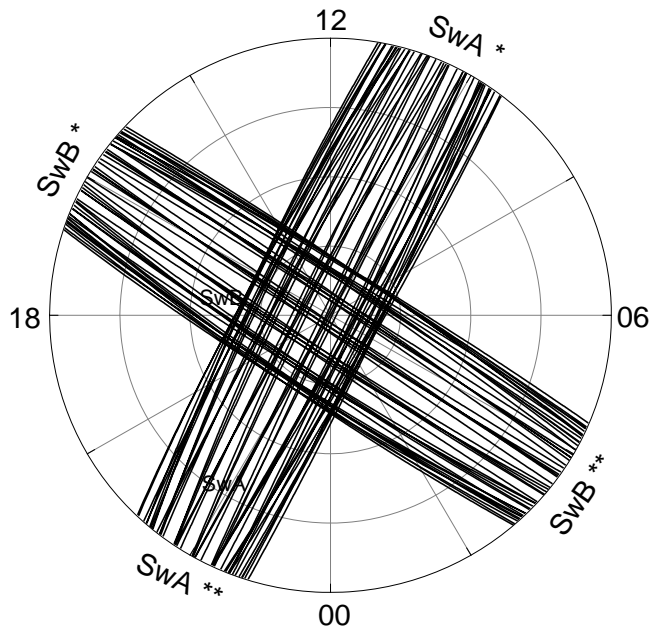


Figure 1: (a) Polar maps of the SwA and SwB orbits on the northern hemispheres on 6-9 September 2017 in the MLT-MLat framework. Circles are drawn every 10° down to 50° MLat. Symbol * and ** indicates 15 the entry and exit point, respectively. **(b)** Daily (UT) variation of MLTs at which SwA and SwB cross the latitude MLat=60° on the northern (blue) and southern (red) hemispheres.

Table 1. MLT range of the tracks in the northern and southern polar regions

Satellite	MLT range within which the satellite cross the boundary of 50° (70°) MLat, (hh:mm)*	Center of the MLT range	
		hh:mm	hh
Northern hemisphere			
SwB	02:50-04:30 (01:30-05:10)	03:40	04
SwA (SwC)	09:20-11:30 (08:40-12:50)	10:30	10
SwB	15:00-16:50 (14:20-18:10)	16:00	16
SwA (SwC)	21:00-22:50 (19:40-23:30)	22:00	22
Southern hemisphere			
SwB	03:10-05:00 (01:50-06:20)	04:00	04
SwA (SwC)	09:10-11:00 (08:30-12:20)	10:00	10
SwB	14:50-16:40 (14:10-18:00)	15:50	16
SwA (SwC)	21:20-23:10 (20:00-23:50)	22:10	22

* with accuracy of 10 min

3 Space weather conditions on 6–9 September 2017

5 At the declining phase of solar cycle 24, starting from 6 September 2017, strong multiple solar flares occurred. The associated interplanetary coronal mass ejections collided with Earth's magnetosphere and caused the most intense magnetic storm of the recent solar cycle. The storm produced strong geomagnetic disturbances, ionospheric effects, magnificent auroral displays, elevated hazards to power systems and unstable HF radio wave propagation (e.g. Chertok et al., 2018; Clilverd et al., 2018; Curto et al., 2018; 10 Yasyukevich et al., 2018).

Evolution of the solar wind (SW) parameters and geomagnetic activity is presented in **Fig. 2** showing (from top to bottom): the IMF B_z and B_y, the SW proton speed (V_{sw}) and density (N_{sw}), the auroral AL and the equatorial SYM-H geomagnetic indices from the OMNI-web service (<https://omniweb.gsfc.nasa.gov/>).

15 Two SW shock events impact the magnetosphere. The arrival of the first shock late on 6 September (23:50 UT) results in a sudden increase in all parameters except the AL index. Since IMF B_z turns northward, this initial disturbance is only weakly geoeffective as a result. At 20:40 UT, 7 September, IMF B_z turns southward that triggers a substorm **growth phase** and a ring current build up. The second shock arrived at

~23:40 UT on 7 September, with the SW speed up to 800 km/s and strongly negative Bz and By. This shock causes an abrupt drop of SYM-H down to -150 nT and a spike-like decrease of AL down to -2200 nT. After 03 UT, 8 September, the IMF Bz becomes positive, AL gradually approaches to zero and SYM-H starts to recover until the next southward turn of Bz. At ~06 UT on 8 September another strongly negative Bz period is seen, and the SW speed remains high (>700 km/s). This causes the second substorm (AL is -2000 nT) and ring current intensification (SYM-H is -100 nT). A steady recovery occurs in the AL index throughout 9 September, while the SYM-H gradually increases from -75 to -35 nT. The SW parameters are not available for this day.

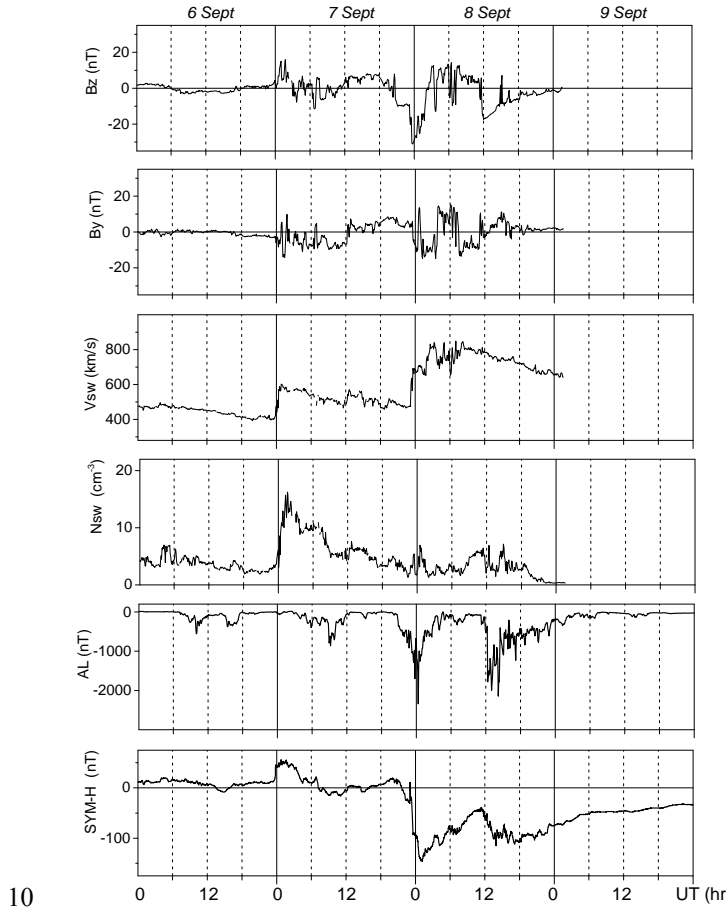


Figure 2: From top to bottom: IMF Bz and By, SW speed and density, AL and SYM-H indices on 6-9 September 2017 (5-min values).

4 Data analysis

4.1 FAC densities

5 Statistically the large-scale R1 and R2 FAC densities are peaked at the dawn-dusk meridian. In this regard, satellites orbits on September 2017 are not optimal for identifying the R1/R2 extremes, since they are deviated from this meridian. However, the local times of satellite paths are representative enough to assess the evolution of these FACs. On dusk, the orbits of SwB are centered at about 16 MLT that is not far from the region, where the current density is expected to be maximal. On the night side, the orbits are centered at 10 04 MLT, where they overlap the ionospheric westward electrojet, which is greatly enhanced when a substorm occurs. SwA and SwC cross the pre-noon sector at about 10 MLT, where both the downward R1 and upward R2 are often identified. These satellites also cross the pre-midnight sector, where disturbances associated with substorms are expected.

15 An example of the FACs measured along the SwB track is shown in **Fig. 3**. The 1 s values of FAC presented in **Fig. 3a** provide clear evidence for strong bursts in the auroral latitudes ($55\text{--}75^\circ$ MLat), while the near-pole region is almost empty of FACs. The auroral FACs exhibit large-amplitude spike-like structures, thus confirming the existence of filamentary current sheets embedded into the large scale current sheets. The intensities of these small-scale FACs vary from units to tens $\mu\text{A/m}^2$. **Fig. 3b** depicts the 21-20 point smoothed curve. It can be seen that the satellite approaching the pole from the dusk observes first the downward (positive) R2 and then the upward (negative) R1 current, both are of $\sim 2 \mu\text{A/m}^2$ density. Above approximately 70° MLat FACs become marginal. When the satellite moves equatorward in the early morning local times, a multi-layer structure is observed, in which the poleward currents are mostly positive, so they may be associated with downward the R1 FAC. The most equatorward currents are negative and 25 thus represent the R2 FAC.

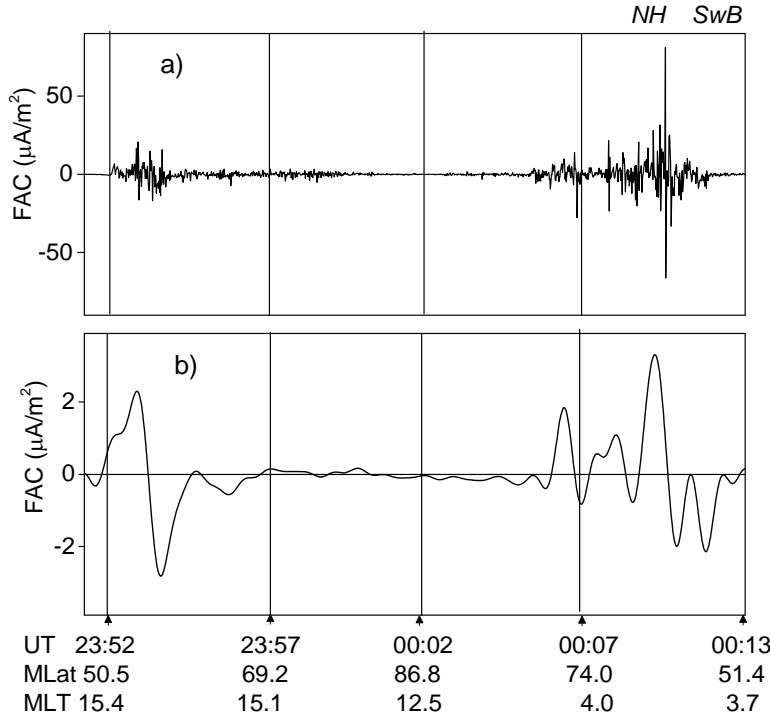


Figure 3: (a) 1 s and (b) smoothed FACs measured by SwB in the northern polar region between 23:50 UT, 7 September, and 00:13 UT, 8 September. Downward (upward) current is positive (negative).

To demonstrate the global temporal evolution of FACs, in **Fig. 4** the current intensities for the four MLT sectors are presented separately for the northern (**Fig. 4 a, c, e, g**) and southern (**Fig. 4 b, d, f, h**) hemispheres. Each red (blue) point is determined by averaging the downward (upward) current densities when the satellite crosses the region filled with FACs. The upper (**a - d**) and lower (**e - h**) plots represent the data from the day side (10 and 16 MLT) and night side (04 and 22 MLT), respectively. For easier visual association of the evolution of FACs with the storm development, the SYM-H and AL indices are added in the plots (**a, b**) representing the day side and in the plots (**e, f**) representing the night side, respectively. During 6-9 September, FACs shown in **Fig. 4**, exhibit three pronounced enhancements, which are of different intensity depending on the MLT sectors. (Note that the FAC densities do not show any systematic changes associated with the orbit oscillation during the day.) All FACs start to increase in the very beginning of September 7 in association with the SW dynamic pressure front impinges the magnetosphere

causing a positive excursion of SYM-H. The dayside FACs increase abruptly (this is especially well seen in **Fig. 4 b - c**, i.e. at 10 MLT, north, and at 16 MLT, south), while the nightside FACs (**Fig. 4 e - h**) respond to the shock with a considerable delay. The nightside FACs are peaked in the middle of September 7, when a moderate substorm occurs.

5 In the very beginning of September 8, in association with the first deep drops of SYM-H and AL, a step-like increase is seen at all MLTs except the prenoon sector. The peak of the day- and nightside FACs reaches 2.5 and 3.5 $\mu\text{A}/\text{m}^2$, respectively. For a particular crossing the average density exceeds 5-6 $\mu\text{A}/\text{m}^2$ as seen from the standard deviation. The dayside FACs (**Fig. 4 a - d**) stay enhanced during the whole day
10 of 8 September. The nightside FACs (**Fig. 4 e - h**) more closely follow the evolution of AL, so that the current intensities decrease in accordance with the first storm-time substorm recovery. The next increase in the nightside FACs occurs at ~12 UT on September 8, when the second major substorm occurs and the second drop in SYM-H is observed. On the day side the response of FACs to this substorm is marginal, although the current densities remain elevated throughout the day. All FACs fall to pre-storm levels by
15 September 9.

Comparison of the evolution of FAC intensity with the SW and geomagnetic parameters during the period of 6-9 September reveals that the storm-time FACs are, on average, by several times larger than the quiet-time ones. Better **correspondence** exists between the nightside FACs (but not the dayside ones) and the
20 substorm activity as monitored by AL index. Although FACs are considerably enhanced during a storm main phase in all MLT sectors, the correlation between the current densities and SYM-H is **not straightforward**. Also **we could not find any** simple relation with any isolated SW input, such as the IMF or the SW dynamic pressure.

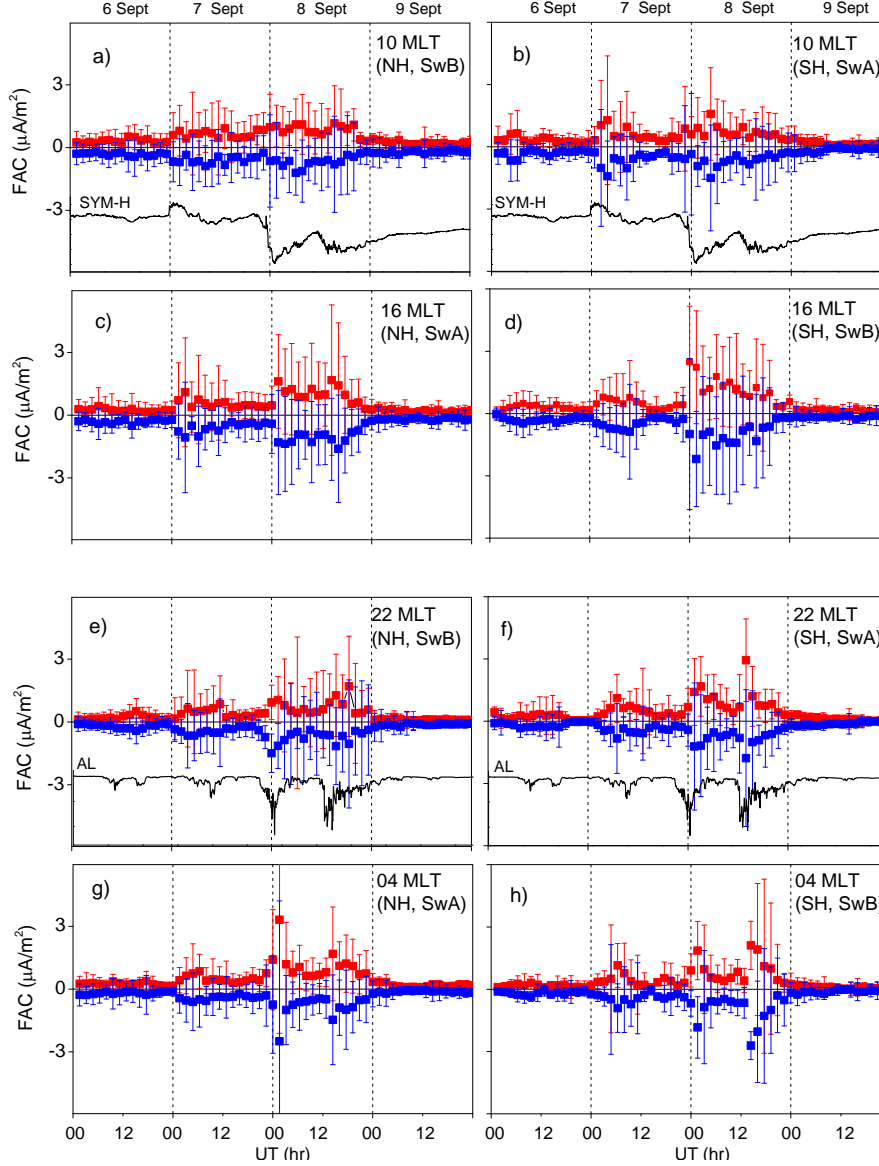


Figure 4: Average FAC densities in the four local time sectors covered by the *Swarm* data on 6-9 September, 2017. The left column of plots corresponds to the northern hemisphere (NH) and the right column corresponds to the southern hemisphere (SH). The upper plots (a-d) and the lower plots (e-h) show the dayside and nightside FACs, respectively. The SYM-H and AL indices are added in the plots (a, b) and (e, f), respectively. The centered MLT (10, 16, 22 and 04) is shown in the right upper corner of each plot. The downward and upward FACs (and the corresponding error bars) are shown in red and blue, respectively.

4.2 Dawn-dusk asymmetry

During the event of September 2017 a signature of the dawn-dusk asymmetry in the storm-time FACs is revealed. Although the estimate is based on a limited number of crossings and does not allow calculating the total FAC, the current densities summed separately over the dawn and dusk sides may serve as a proxy. Those parts of the tracks which fall into the 00-12 MLT (12-00 MLT) sector are considered to be related to the dawn (dusk) side, MLat for 50° – 90° is accounted. The summed up- and downward FAC densities in each MLT sector as well as those for dawn and dusk sides are presented in **Table 2**. The summation is over the entire 4-day interval.

10 For any given pass, the net summed FAC density is frequently nonzero. As seen in **Table 2** the net FACs summed in a particular MLT range, is also nonzero. The difference between upward (negative) and downward (positive) current densities varies from 1 to 15%. For the sectors centered at \sim 04 and 10 MLT this difference is relatively small (-0.7 and $+0.1 \mu\text{A}/\text{m}^2$ in the Northern hemisphere, and $1.6 \mu\text{A}/\text{m}^2$ and $-0.4 \mu\text{A}/\text{m}^2$ in the Southern hemisphere), i.e the R1 and R2 densities are of comparable values. For the sectors centered at 16 and 22 MLT the downward (R2) FACs exceed the upward (R1) FACs by $5.2 \mu\text{A}/\text{m}^2$ and $3.1 \mu\text{A}/\text{m}^2$ in the Northern hemisphere, and by $3 \mu\text{A}/\text{m}^2$ and $3.4 \mu\text{A}/\text{m}^2$ in the Southern hemisphere.

20 If the MLT sectors are combined in pairs in order to obtain FACs summed over the dawn and dusk sides, the prevalence of the dusk-side downward current is revealed. From the values presented in the two last columns of **Table 2** one can see that on both hemispheres the duskside downward current ($+60$ and $+58.9 \mu\text{A}/\text{m}^2$ on the Northern and Southern hemisphere, respectively) is stronger than all the other currents. Although the numbers in **Table 2** contain uncertainties related to the lack of global observations, the estimate based on the summed FAC densities from in-situ *Swarm* measurements indicate the existence of 25 the storm-time dawn-dusk asymmetry. Even a limited number of crossings show a clear tendency of the prevalence of the dusk-side R2. This predominance implies an additional amplification of the storm-time R2 FAC on the dusk side, which is related to the partial ring current. This shift may result from a strong dusk side ion pressure leading to asymmetric dusk-side inflation of the magnetic field consistent with a partial, dusk side, ring current during storm main phase (Liemohn et al., 2001; Anderson and Korth, 2007).

Table 2. Summed upward (negative) and downward (positive) FAC densities in for all passes on 6-9 September. In the last two columns the conventional FAC regions (R1 or R2) are indicated in brackets. The largest values are shown in bold.

5

Side	MLT range (as at 50° MLat) *	FAC densities ($\mu\text{A}/\text{m}^2$)			
		up	down	up	down
Northern Hemisphere					
dawn	09:20 – 11:30	-23.3	+23.4	-54.6 (R2)	+53 (R1)
	02:50 – 04:30	-31.3	+29.6		
dusk	21:00 – 22:50	-27	+30.1	-52.7 (R1)	+60 (R2)
	15:00 – 16:50	-24.7	+29.9		
Southern Hemisphere					
dawn	09:10 – 11:00	-27.8	+27.4	-51.5 (R2)	+52.7 (R1)
	03:10 – 05:00	-23.7	+25.3		
dusk	21:20 – 23:10	-23.8	+27.2	-52.5 (R1)	+58.9 (R2)
	14:50 – 16:40	-28.7	+31.7		

* with accuracy of 0.5 hr

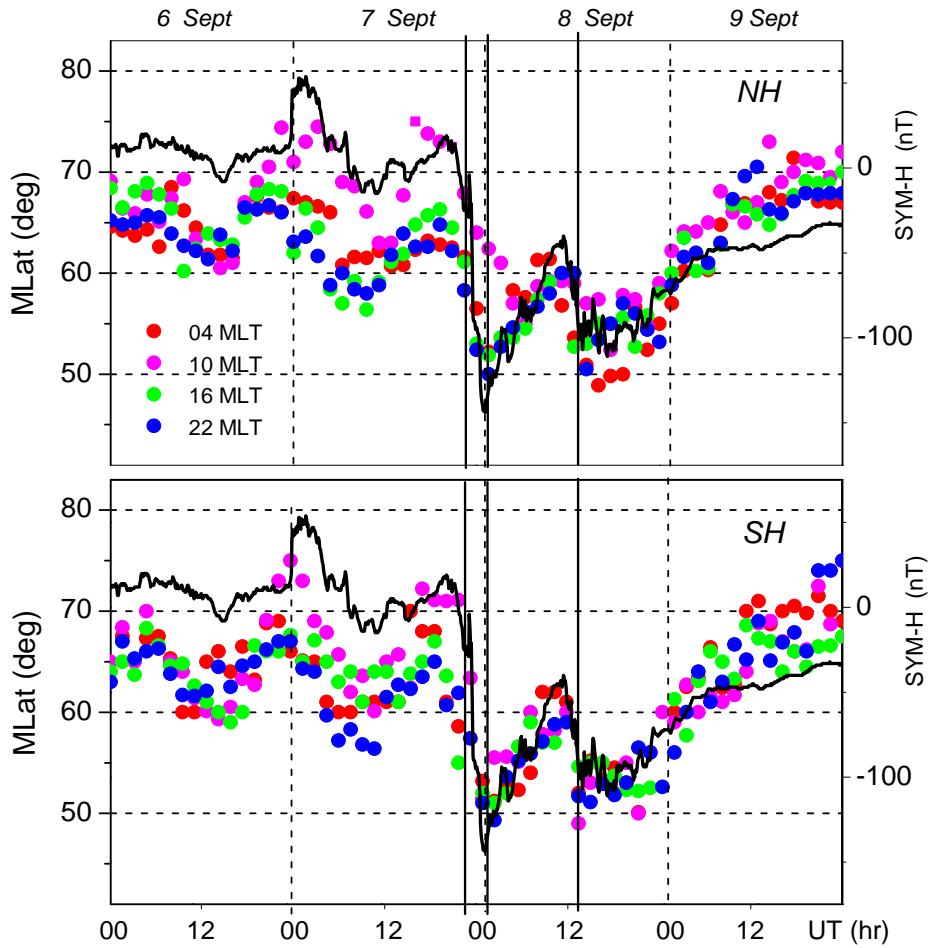
4.3 Dynamics of the equatorward boundary of the FAC region

10 It is well established that the enhanced SW input and the pile-up of open magnetic flux during a geomagnetic storm results in the equatorward expansions of the polar cap and the auroral oval as a whole (e.g. Milan et al., 2004). Following the magnetospheric dynamics FACs also move equatorward. **Fig. 5** shows the evolution of the equatorward boundary (EqB) of FACs on 6-9 September. For easier comparison the SYM-H index is added to each plot. The EqB parameter is determined as the lowest MLat at which 15 FACs are terminated. The procedure of the 20-point sliding window (the scale is about 150 km) moving along a track from the equator to the pole is applied to the 1 s FAC values and the corresponding MLats. EqB is selected as the lowest MLat of the window if 90% of FAC values within the window exceed $|0.1| \mu\text{A}/\text{m}^2$. Then the results are checked visually in order to avoid the erroneously calculated latitudes, that may happen, e.g., if a significant latitudinal gap between R1 and R2 occur. When calculating EqB, no 20 separation between the up- and downward FACs is made.

Even visual comparison of the SYM-H and EqB evolutions in **Fig. 5** reveals generally coherent behavior of these two parameters. In particular, during a period preceding the storm main phase (before 8 September, when SYM-H is mainly positive) EqB is located much lower than during the end of recovery phase (after ~12 UT on 9 September, when SYM-H is still negative). Before the SYM-H attains its stable negative values <-20 nT at 22:00 on 7 September FACs are observed mainly poleward of 60° MLat on both hemispheres. Moderate equatorward shifts of EqB are associated with the modest substorms occurred before the storm main phase in the middle of 6 and 7 September. Prior the main phase, on both hemispheres the prenoon (04 MLT) EqB is found considerably poleward compared to the EqB location at other MLTs. The effect is well seen during the two time intervals: from ~22 UT, September 6 till 06 UT, September 7 and at 12-24 UT, September 7. Both intervals are dominated by the northward IMF (sf. **Fig. 2**), so that a shrinking of the polar cap and a poleward shift of the auroral oval is expected. With regard to the position of FACs, the displacement of its equatorward boundary is the largest only in the pre-noon sector, while the other local times remain less affected.

Upon arrival of the SW shock at the very end of September 7, EqB is abruptly shifted equatorward, then tends to recover until the middle of September 8, and then drops again following the second intensification of the storm. At the very beginning of 8 September EqB is found at its lowest position at 50° MLat. A drop of EqB occurs simultaneously with the peak of the first storm-time substorm just between 7 and 8 September and with the lowest SYM-H (below -150 nT). The second substorm reaches its peak slightly before the second minimum of SYM-H (at 12:50 and 13:55, respectively). During this second activation the EqB is shifted again as low as 50° MLat (although SYM-H is only -100 nT). As seen in **Fig. 5**, the evolution of EqB tends to follow the gradual change of SYM-H rather than an abrupt drops of AL related to the substorm onset (see also **Fig. 2** for AL). Unlike the nightside current density, which exhibits several spike-like increases in accordance with AL and the dayside density, which is enhanced throughout the storm, temporal variations of EqB are relatively smooth and tend to follow the SYM-H index. In the end of September 9, during the late recovery phase of the storm, EqB is shifted poleward as high as 70° MLat. As far as the day-night asymmetry is concerned, almost no difference in evolution on the day- and nightside EqBs is observed during the main and recovery phases. Because the storm-time substorms are relatively

short-lived, an expansion of the FAC region during the growth phase, and then a contraction are difficult to resolve with the *Swarm* data.



5 **Figure 5:** Magnetic latitude of the FAC equatorward boundaries on the Northern (top) and Southern (bottom) hemispheres for the sectors centered at around 04, 10, 16 and 22 MLT (MLat for each individual MLT sector is shown by dots of different colors). The SYM-H index (black line) is superimposed on MLat. Three vertical solid lines mark successively the beginning of the storm main phase at 22:00 on 7 September (the time when SYM-H attains its stable negative values <-20 nT), the peaks of the first and second major substoms (the time when AL attains its
10 minimum)

4.4 Small-scale FACs

It is known that FACs appear on a wide range of scales from large-scale sheet-like currents of hundreds kilometers width to very small-scale filamentary currents of hundreds meters width. The quasi-instantaneous amplitudes of the small-scale component are often much larger than the stationary R1/R2 5 FACs. The current intensity vary inversely with scale so that large-scale currents are typically a few $\mu\text{A}/\text{m}^2$, whereas the smaller scale (down to 10 km) are a few tens $\mu\text{A}/\text{m}^2$ (Neubert and Christiansen, 2003; Luhr et al., 2015; McGranaghan et al., 2017). To obtain the time-series of the *Swarm* peak current densities on 6-9 September 2017, the largest positive and negative 1 s values were selected from each crossing in a given 10 MLT time sector irrespective of the hemisphere. The obtained peak values are presented in **Fig. 6**. First of all, from this figure one can see that the small-scale peaks may be more than an order of magnitude larger 15 than the FACs averaged over a track (sf. **Fig. 4**). On September 6, only two outliers of about $+20 \mu\text{A}/\text{m}^2$ and $-30 \mu\text{A}/\text{m}^2$ are observed. Both are from the pre-midnight sector and are associated with a moderate 20 substorm occurred in the middle of this day. During the disturbed period, starting with the compression of the magnetosphere on September 7, the amplitude of peaks tends to increase. Two intense substorms occurring during the storm main phase cause an additional strengthening of small-scale FACs at all MLTs. At ~00 UT on September 8, the up- and downward currents located in early morning local times attain their extremes of $70\text{-}80 \mu\text{A}/\text{m}^2$. The second major substorm occurred in the middle of September 8 is also accompanied by the peaks, which are more pronounced in the dusk-side, where the upward FAC reaches about $-50 \mu\text{A}/\text{m}^2$. Note that some peaks can be missed due to the temporal and spatial gaps between the satellite tracks.

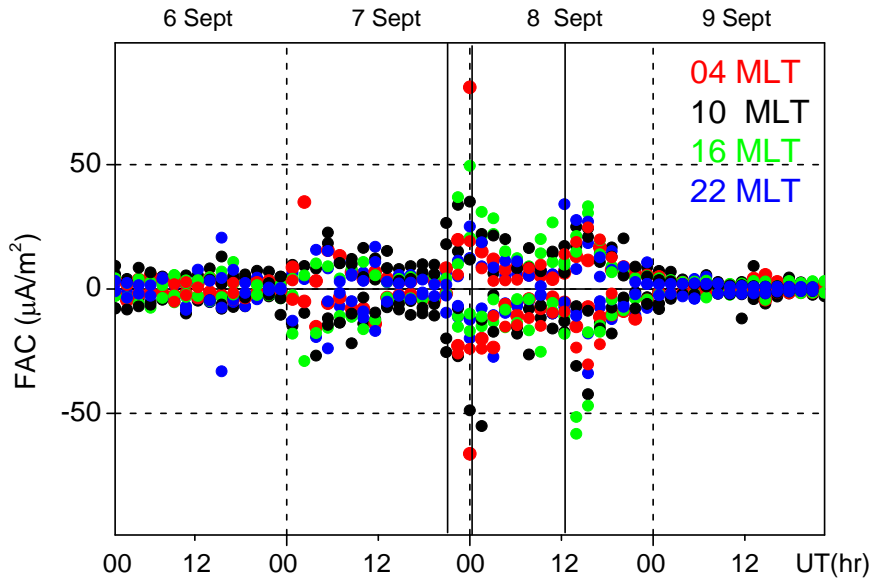
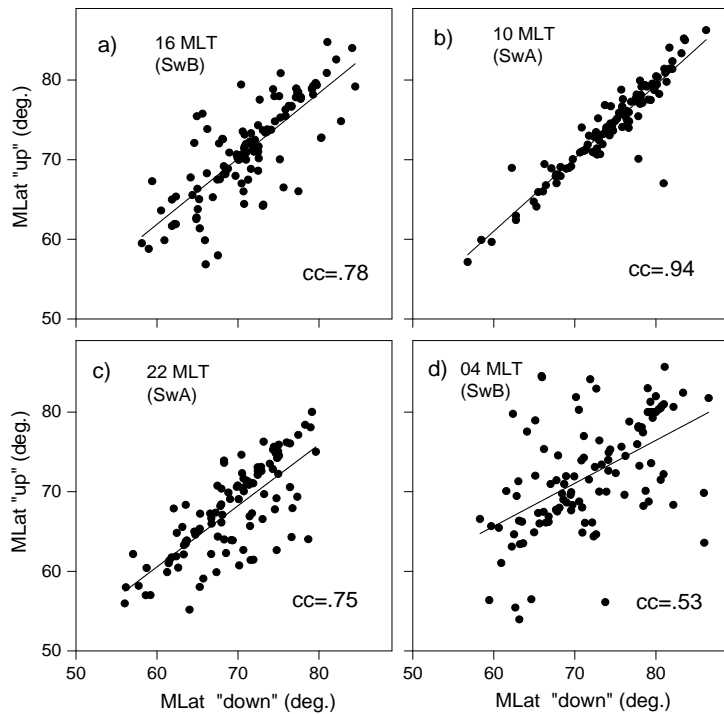


Figure 6: The largest downward (positive) and upward (negative) 1 s current densities for four MLT sectors on 6-9 September. The vertical solid lines mark the beginning of the storm main phase at 22:00 on 7 September (the time when SYM-H attains its stable negative values <-20 nT), the peaks of the first and second major substoms (the time when AL attains its minimum)

When for each crossing within a certain MLT sector, the minimum (i.e. peak upward current) and the maximum (i.e. peak downward current) 1 s FACs are selected, it appears that in some cases these peaks are observed at very close latitudes, while in other cases the minimum and maximum are spaced in latitude. In Fig. 7, the correlations between the MLats, at which the most intense small-scale FACs of opposite polarities are observed, are presented for each MLT sectors. The x-axis (y-axis) corresponds to the MLat of the downward (upward) peak selected in each crossing. The magnitude of minima and maxima are not accounted. From Fig. 7 one can see that correlation between the latitudinal positions of the up- and downward peaks varies with MLT. The highest correlation coefficient ($cc=0.94$) is found in the pre-noon sector (Fig. 7b). This is indicative of a large population of the paired, closely adjacent small-scale currents of opposite polarity (called hereafter the bipolar structure). In the dusk (Fig. 7a) the correlation coefficient decreases down to 0.78. Almost the same correlation ($cc=0.75$) is observed in the pre-midnight sector (Fig. 7c). At the early morning hours (Fig. 7d) the correlation is much weaker ($cc=0.53$) implying that the

extreme up- and downward currents appear less frequently in pair but rather are spatially (or temporary) separated. Different mechanisms of the small-scale FAC formation on the day- and night side can be the cause of this spatial distribution and variability.



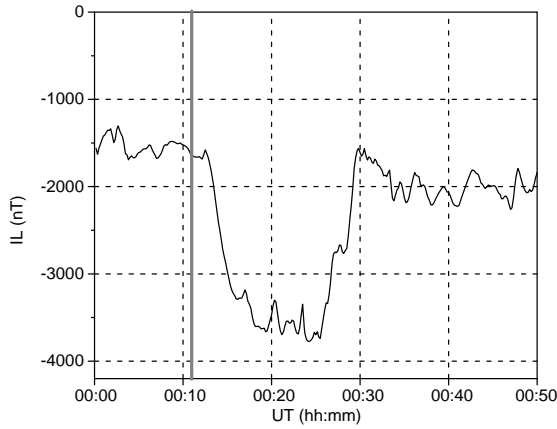
5

Figure 7: Correlations between magnetic latitudes, at which the up- and downward peak FACs are observed: **(a)** dusk, 16 MLT; **(b)** pre-noon, 10 MLT; **(c)** pre-midnight, 22 MLT; **(d)** post-midnight/early morning, 04 MLT.

4.5 Small-scale FACs of extreme amplitudes

10 During the storm under consideration a pair of the most intense upward and downward small-scale FACs is revealed by SwB at around 00:10 UT on September 8, when the satellite traverses the auroral latitudes from north to south over the geographic area of the Barents Sea, about 20 degree magnetic longitude to the East from the IMAGE magnetometer network (<http://space.fmi.fi/image>). The network produces the IL index, which is simple estimate of the total westward currents crossing the IMAGE chain. The IL index (**Fig. 8**)

shows that the extreme FACs are observed during the growth phase of the first storm-time substorm, several minutes before the IL drops below -3500 nT.



5 **Figure 8:** The 10 s IL index at 00:00-00:50 UT, September 8. Time of the extreme FAC observation is shown by thick
grey line.

The 1 s FACs and plasma parameters (the electron density, N_e , temperature, T_e , and the spacecraft electric

potential, U_{sc}) measured by SwB at 00:08-00:12 UT on 8 September are shown in **Fig. 9**. As show in **Fig.**

10 **9a**, at 00:10:18-00:10:19 UT the satellite observes the bipolar current structure of extreme density
consisting of the poleward downward ($81 \mu\text{A}/\text{m}^2$) and equatorward upward ($-66 \mu\text{A}/\text{m}^2$) FACs. The paired
up- and downward FACs are of comparable values, thus they are balanced and likely closed locally. In **Fig.**
9a the original 1 s values are superimposed to the smoothed curve, which reveals that the bipolar structure
is located just between the large-scale downward (R1) and upward (R2) FACs.

15

The bipolar current structure is accompanied by plasma perturbations. A narrow peak in N_e up to $77 \cdot 10^3$

cm^{-3} (**Fig. 9b**) and an increase of T_e up to $\sim 10^4$ K on average (**Fig. 9c**), that is $\sim 50\%$ above their ambient

values, are observed almost simultaneously with a pair of extreme FACs. (It should be noted that the T_e

20 values presented here are based on the current processing of the satellite data and may be still uncalibrated.

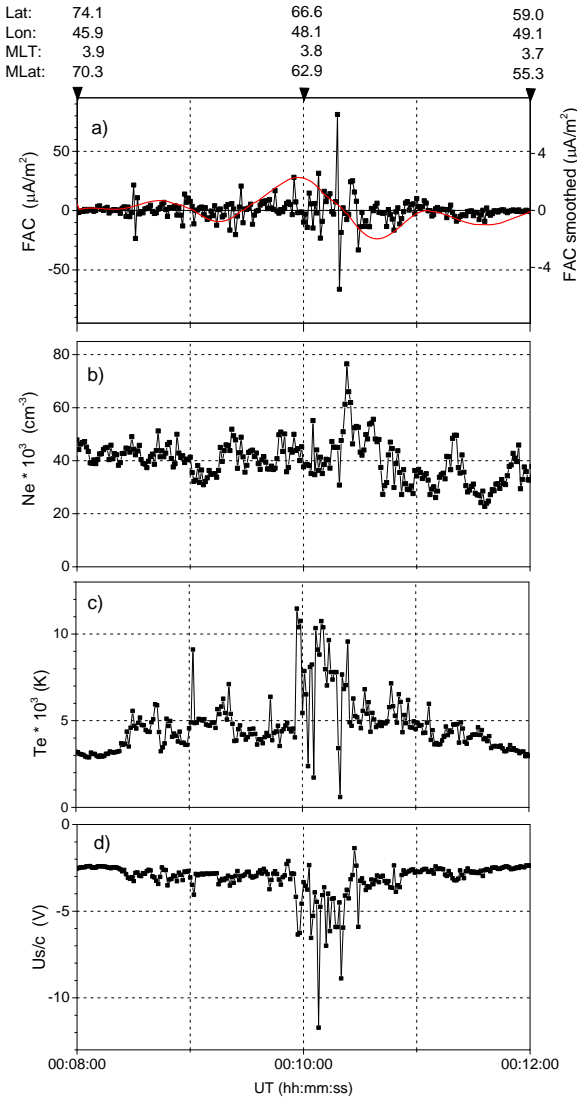
However, it hardly affects the relatively small-scale perturbations.) The elevated T_e is observed in a wider
region slightly poleward of the enhanced N_e . The plasma disturbances are clearly seen in U_{sc} , which is

proportional to $-k \cdot T_e$ (k is the Boltzmann constant). Note that the level of noise for the U_{sc} channel is much lower compared to that for the T_e channel (0.4% and 2% for U_{sc} and T_e , respectively). **Fig. 9d** shows that a reduction of U_{sc} starts at 00:09:56 UT, then peaks at 00:10:08 (-12 V) and 00:10:20 UT (-8 V), the average decrease is -5 V. The region, where the T_e and U_{sc} are perturbed is several times wider than region 5 occupied by the pair of extreme FACs..

If the localized increase in N_e indicates conductance enhancement (likely due to precipitating electrons), the observed plasma and current perturbations are similar to those associated with auroral arcs (Opgenoorth et al. 1990; Lyons, 1992; Lewis et al., 1994; Johnson et al., 1998; Aikio et al., 1993; Juusola, et al., 2016). 10 In particular, Aikio et al. (2002) studied the current system of arcs in the evening sector, where the background electric field is northward. It was shown that for arcs located within the northward convection electric field currents flow downward on the equatorward side of the arcs, then poleward, and upward from the arcs. The arcs are associated with an enhanced northward-directed electric field region on the equatorward side of the arc. An enhancement in the electric field starts already several tens km 15 equatorward of the arc edge.

During the storm under consideration the bipolar FAC pattern observed at 00:10 UT is located in the morning sector, where the background electric field is expected to be southward. This is confirmed by the SuperDARN-based convection model (<http://vt.superdarn.org/tiki-index.php?page=ASCIIData>), which 20 predicts in the region of the SwB observations the magnitude of the southward and westward component of about 6.5 mV/m and 0.5 mV/m, respectively. **As mentioned in Section 2.1, unfortunately the in-situ *Swarm* electric field is unavailable. Only the reported characteristics of the electric field associated with arcs can be used for qualitative analysis.** In particular, for morning side arcs an enhanced southward electric field on the poleward side of the arc is expected. In this case the current pattern consists of a downward FAC on the 25 poleward side of the arc connected to an upward current above the arc by an equatorward ionospheric closure current. This is exactly what is seen in **Fig. 9a**: when SwB flies away the pole, it first observes a positive spike (downward FAC) and then a negative spike (upward FAC). Since the width of the region of enhanced N_e is ~ 30 km, the arc is relatively narrow. Comparing **Fig. 9a** and **Fig. 9b** one can see that the paired FACs is located on the poleward side of the region of enhanced N_e . Note, that in **Fig. 9b** a sharp 30 increase in N_e up to $\sim 80 \cdot 10^3 \text{ cm}^{-3}$ is preceded by a weaker spike-like drop down to $\sim 30 \cdot 10^3 \text{ cm}^{-3}$. A

decrease in Ne (which is usually much less pronounced than an **increase** due to precipitating electrons) is associated with a downward FAC observed at the opposite boundary of the arc. Elevations of Te **may be** created by electric fields which can arise within narrow region adjacent to the northern side of the auroral arc **as observed by Aikio et al. (2002)**.



5

Figure 9: The 1 s values of (a) FAC density, (b) Ne , (c) Te , and (d) Us/c measured along the SwB track at 00:08:00 – 00:12:00 UT, 8 September. In the upper plot the 21-point smoothed FAC density is also shown. Geographic and geomagnetic coordinates are shown on the top.

5 Discussion

Observations of the LEO *Swarm* multi-satellite mission are used in order to identify various characteristics of the storm-time FACs for the severe event of 6–9 September 2017. During the storm main phase two major substORMS occurred, so that the FAC system evolved under conditions of the storm-substORM interplay. In mid-September 2017 the separation between the upper and lower *Swarm* satellites was about 6 hours in local time. Within the sectors centered at 04, 10, 16 and 22 MLT the northern and southern polar regions were covered by about 60 tracks along which the 1 Hz measurements of FACs were carried out. These observations made it possible to reveal the evolution of the large scale FAC intensities, the displacement of the FAC equatorward boundaries and the some features of the extreme small-scale FACs.

5.1 Large-scale FACs

Evolution of large-scale FACs during the September 2017 storm is in general agreement with regularities observed previously by *CHAMP* during the intense 2003 geomagnetic storms (Wang et al., 2006). The common feature of all storm-times is the equatorward motion of FACs generally correlating with the storm intensity. During the September 2017 storm the global coverage of the high latitudes by the precise measurement onboard of *Swarm* satellites made it possible to reveal that the FACs was enhanced at all MLTs starting from the time of the first SW shock arrival at the very beginning of 7 September, although the northward IMF and the prolonged period of geomagnetic quietness lasted almost a day. After this quietness a storm abruptly commenced at ~22: UT on 7 September. During the two-step main phase FACs exhibit three pronounced enhancements, the evolution of FACs depends on the MLT sectors. On the dayside FACs strengthen after the sudden commencement and in response of the first drop of SYM-H, while the response to the second drop of SYM-H is relatively weak. On the night side the current intensities follow mainly the substORM dynamics as monitored in terms of the AL index, promptly respond to the onset of storm-time substORMs and strengthen at the peak of substORM. At the same time, during the period between the major substORMs, when AL is fully recovered, but SYM-H is not, FACs stay considerably enhanced.

The September 2017 storm is characteristics of a considerable equatorward expansion of the FACs region as low as 50° MLat on both hemispheres. The latitudinal displacement of FACs is more gradual and smooth compared to the changes in current intensity. For comparison, during the 2003 storms the minimum latitude of peak current density are limited to 52-56° MLat (Wang et al., 2006). It should be noted that 5 Wang et al. (2006) defined the latitudinal positions of peak current density but not the most equatorward boundary of the FAC region, thus the actual FAC region may expand to lower latitudes. Similar to the 2003 storms, in 2017 the latitudinal positions of EqB generally follow the SYM-H index variation. FACs are shifted further equatorward during the storm-time substorms. Even a relatively minor substorm occurred prior the storm causes a considerable equatorward displacement of FACs. The lowest latitude of EqB is 10 observed when both the SYM-H and AL indices reach their minimums.

Although the 2017 storm is considerably weaker ($Dst \approx -100$ nT) than the 2003 ones ($Dst \approx -400$ nT), in the 2017 event, the FACs are expanded to approximately the same latitudes. This effect may be interpreted in terms of saturation, when the FAC region does not expand lower than ~50° MLat independent of the storm 15 severity. Linear dependence between latitudinal boundaries of the FAC sheets upon the dayside merging electric field, the AE and Dst indices has been reported by Xiong et al. (2014). It was pointed out that toward high activity a saturation of equatorwards expansion seems to set in.

In September 2017, prior the storm main phase, when the IMF B_z is northward, the pre-noon EqB is 20 located at higher latitudes (~75° MLat) compared to the other MLT sectors (~65 MLat). Surprisingly, in the course of the storm main phase, no considerable difference between the latitudinal positions of EqB in different MLT sectors is found. After ~12 UT on September 9, in the late recovery phase (SYM-H is still -50 nT), both the day- and nightside EqB recover to undisturbed position (about 70° MLat). The coherent behavior of EqB is rather unexpected because Wang et al (2006) found that the poleward recovery of FACs 25 on the nightside is slower than on the dayside. Previous analysis of the latitudinal shift of the polar cap boundaries based on the *IMAGE* observations during a magnetic storm has also shown that, if the IMF B_z turns northward, the dayside boundary recovers much faster than the nightside boundary (Lukianova and Kozlovsky, 2013). This is because dynamics of the nightside boundary depends on the energy accumulated in the magnetotail during the previous period of the storm main phase. However, it seems that the storm of 30 September 2017 does not show the same regularity. The reason may be that during the storm main phase

the two major substorms occurred, so that the energy stored in the tail was released faster. Comparing the evolution of the FAC densities and the equatorial boundary positions during the storm recovery, one can see that the densities decay much faster than the boundaries return to their quiet time positions.

5 The *Swarm* observations, although they are instantaneous, reveals the dawn-dusk asymmetry FACs. The dawn-dusk asymmetry is revealed by comparing the up- and downward FACs, which are summed separately over dusk and dawn. While the summed FAC intensities are comparable between the two hemispheres, the positive and negative densities on the dusk and dawn are slightly imbalanced and the net current is nonzero. It seems that the dusk-side downward (R2) FACs considerably exceeds the dusk-side
10 R1 and the dawn-side R1/R2 currents. The observed imbalance in FACs is likely related to an intensification of partial ring current, which is connected to R2 FAC on the dusk. Strengthening of partial ring current may also lead to asymmetric dusk-side inflation of the geomagnetic field lines. The dawn-dusk asymmetry in strength and the equatorward displacement of R1 and R2 at the peak of the major storm on August, 2000, has been reported by Anderson and Korth (2007). This study was utilized the global
15 distributions of FACs generated at a 10 min cadence separately for the Northern And Southern Hemisphere by the AMPERE project which is based on the fleet of Iridium satellites. For the storm of September 2017 almost no difference in the equatorward shift of the dusk and dawn side FACs is observed. In accordance with the previous observations the dawn-dusk asymmetry is rather manifested in the enhanced density of R2 FAC on the dusk side.

20 5.2 Small-scale FACs

Due to their large amplitudes small-scale FACs play an important role for the energy input to the upper atmosphere. In several previous studies, the FACs associated with arcs were estimated as 1-10 $\mu\text{A}/\text{m}^2$ (Bythrow and Potemra, 1987; Elphic et al., 1998; Janhunen et al., 2000; [Luhr et al., 2016](#)). Larger range of current densities, varying between 4 and $>40 \mu\text{A}/\text{m}^2$, has been observed (Aikio et al., 2002) and even more
25 intense small-scale FACs, up to hundred of $\mu\text{A}/\text{m}^2$, at the edges of arcs have been measured by MEO satellites (Marklund et al. 1982; Bythrow et al. 1984). Such a large range of the FACs estimates is likely related to its different scales (and different techniques), because for arcs with very sharp electron density gradients, the FACs associated with ionospheric currents flow in narrow regions at arc edges. If the real widths are smaller, the current densities are expected to be larger.

Filamentary structures of high densities are always presented in the *Swarm* observations. This implies that a substantial fraction of R1/R2 currents is composed of many small-scale FACs. The narrow high-density currents are averaged out when integrated over a FAC region, so that multilayer structures of steady large-scale FACs depicted by Iijima and Potemra (1978) can be revealed after a proper smoothing. From a statistical study of the temporal and spatial-scale characteristics of different FAC types derived with the *Swarm* satellites Luhr et al. (2015) have shown that small-scale, up to some 10 km FACs are carried predominantly by kinetic Alfvén waves. A persistent period of small-scale FACs of order 10 s, while large-scale FACs can be regarded stationary for more than 1 min. Neubert and Christiansen (2003) studied the morphology of very small-scale FACs from a survey of *Oersted* satellite 25 Hz data. These FACs are distributed in a broad region around the pre-noon and cusp region, and in the pre-midnight sector. It was found that at the considered time scale, instantaneous currents may reach the largest values up to 1000 $\mu\text{A}/\text{m}^2$, while the average current densities reach a maximum of 10 $\mu\text{A}/\text{m}^2$. McGranaghan et al. (2017) demonstrated a local time dependence in the relationships between large (>250 km) and small FAC scales (10–150 km width, density is up to 0.5 $\mu\text{A}/\text{m}^2$). It was found that linear relationships exist near dawn and dusk local times, while at noon and midnight local times no similar regularity is seen. The results are based at all available data from the *Swarm* satellites and the AMPERE irrespective of the level of geomagnetic activity.

During the September 2017 storm one of the *Swarm* satellites managed to observe a pair of the most intense small-scale 7.5 km width FACs of opposite polarity, the magnitude of which are approximately +80 and -70 $\mu\text{A}/\text{m}^2$. These up- and downward FACs are adjusted to each other and separated in a fraction of degree in MLat. The bipolar FAC structure occurs in the region between R1 and R2, just prior of the substorm onset in the vicinity of the newly developed ionospheric WEJ. The polarity reversal captured by the *Swarm* data for two consecutive seconds implies a quite localized current closure through the ionosphere mostly via Pedersen horizontal currents. Although without optical and electric field data one could not make a strict conclusion, the small-scale bipolar FAC pattern accompanied by a localized enhancements in Ne and Te are likely associated with mesoscale discrete aurora. One-to-one correspondence of small-scale FACs with localized electron precipitation events has been previously observed (e.g. Fukunishi et. al., 1991). The SwB observations are in agreement with the disturbances

expected for the acrs occurred on the morning side, where the ambient electric field is southward. The observed features are resemble to those reported by Kozlovsky et al (2007) and Aikio et al. (2002) but bearing in mind that the latter are related to the evening sector, where the background electric field is northward. Based on *Swarm/THEMIS* ASI observations Wu et al. (2017) has associated multiple auroral arcs with up/down current pairs. For these arcs unipolar and multipolar FAC systems with current densities of about a few $\mu\text{A}/\text{m}^2$ have been observed. Arcs in unipolar FAC systems have a typical width of 10–20 km and a spacing of 25–50 km. Arcs in multipolar systems are wider and more separated. In the bipolar structure of extreme intensity observed by SwB in September 8, the current density exceeds the values observed by Wu et al. (2017) at least by a factor of ten, while the spatial extend of FACs is smaller. This difference implies to the existence of sharp electron density gradients at arc edges. Usually, the arcs consist of auroral rays and bright spots moving along the arcs and these spatial irregularities may produce the extreme small-scale FACs. **This study has shown that under disturbed conditions, FACs forming the arc current system may reach hundred of $\mu\text{A}/\text{m}^2$ on the spatial scale of less than ten kilometers.**

15 Statistically, the bipolar structures dominate in the pre-noon. In the post-midnight MLTs they are observed less frequently. While the interpretation of the bipolar structure in the terms of the meso-scale arc pattern seems reasonable, the small-scale FACs are often a result of reconnection processes distributed over the dayside magnetopause and even in the tail for negative B_z . In contrast to the post-midnight, in the pre-noon sector, where cusp/cleft currents are expected, the bipolar structures are quite frequent. This may be a
20 signature of the plasma injections which are accompanied by pairs of FACs generated due to flux transfer event (FTE) formation (Southwood, 1987) or multiple reconnection at the magnetopause. Magnetic topologies associated with FTEs were previously observed by the MEO satellites (Marchaudon et al., 2004; 2006; Pu et al., 2013). The small-scale field-aligned currents are possibly a consequence of turbulence and instabilities associated with the process of opening previously closed magnetospheric field lines and
25 merging them with the interplanetary magnetic field (Watermann et al., 2009). The regularity presented in **Fig. 7** shows that during the September 2017 magnetic storm the bipolar structures dominate exactly in the region where the signatures of FTEs and the reconnection lines formed at the magnetopause are expected. At the same time, a pair of the most intense FACs is observed on the night side.

6 Conclusion

Characteristics of FACs inferred from the 1 Hz *Swarm* observations during the severe magnetic storm of 6-9 September 2017 are presented. This storm is the two-step one with about 22-hr preliminary phase and the intense substorms occurred in the course of the storm main phase. The satellites cross the pre-midnight, 5 pre-noon, pre-dusk and pre-midnight sectors. The following features of the storm-time FACs are found.

Evolution of the current intensities and the latitudinal position of the equatorward boundaries of the FAC region are mainly controlled by a storm-substorm interplay. **The FACs become enhanced starting from the SW shock arrival despite of the prolonged period of the northward IMF.** The night-time FAC densities

10 primarily follow the substorm development while the dayside FACs are intensified in response to the SW shock and then stay enhanced. At the peak of substorm, the FAC densities averaged over a track within a given MLT sector, reach $3 \mu\text{A}/\text{m}^2$, while the undisturbed level is about $0.2 \mu\text{A}/\text{m}^2$. The dawn-dusk asymmetry is manifested on the enhanced dusk side downward (R2) FAC on both hemispheres.

15 The equatorward displacement of FAC sheets (in the north and south and at all MLTs) correlates with the storm intensity as monitored by the SYM-H index. The minimum latitude of the equatorial FAC boundaries is limited to 50° MLat. Displacement of FAC sheets is more gradual and occurs with a considerable time delay compared to the changes in current intensity.

20 The filamentary structures of high-density FACs are always presented in the *Swarm* observations. A bipolar structure (i.e. the adjacent upward and downward small-scale FACs), $\sim 80 \mu\text{A}/\text{m}^2$, 7.5 km width, is observed in the vicinity of the newly developed westward electrojet just prior the substorm onset. Simultaneous plasma perturbations indicate that the FAC pattern is likely associated with mesoscale auroral arc.

Data availability: The data used for the publication of this research are freely available from the *Swarm* Science Team web site (<ftp://swarm-diss.eo.esa.int>). Data selected for the analysis are available upon request (RL).

Competing interests: The author declare that she has no conflict of interest concerning this paper.

5

Acknowledgement

Swarm data are available through the European Space Agency Online platform (<ftp://swarm-diss.eo.esa.int>), after registration. We acknowledge the *Swarm* Science Team for providing the level 2 data and the *Swarm* visualization tool (<https://vires.services/>). The OMNI data on the solar wind, interplanetary magnetic field and geomagnetic indices are obtained from NASA/GSFC's Space Physics Data Facility's CDAweb service (<http://omniweb.gsfc.nasa.gov/>).
10 This research was partly supported by the RFBR (grant 17-05-00475).

References

15 Aikio, A.T., Opgenoorth, H.J., Persson, M.A.L., and Kaila, K.U.: Ground based measurements of an arc-associated electric field, *J. Atmos. Terr. Phys.*, 55, 797–808, 1993.

Aikio, A.T., T. Lakkala, A. Kozlovsky, and Williams, P.J.S.: Electric fields and currents of stable drifting auroral arcs in the evening sector, *J. Geophys. Res.*, 107(A12), 1424, doi:10.1029/2001JA009172, 2002.

Akasofu, S.-I.: The development of the auroral substorm, *Planet. Space Sci.*, 12, 273–282, 1964.

20 Anderson, B. J., S.-I. Ohtani, H. Korth, and A. Ukhorskiy, Storm time dawn-dusk asymmetry of the large-scale Birkeland currents, *J. Geophys. Res.*, 110, A12220, doi:10.1029/2005JA011246, 2005.

Anderson, B.J., and Korth, H.: Saturation of global field aligned currents observed during storms by the Iridium satellite constellation, *J. Atmos. Solar-Terr. Phys.*, 69, 166–169, 2007.

Axford W.I.: Viscous interaction between the solar wind and the Earth's magnetosphere. *Planet. Space Sci.* 12 ,45, 25 1964.

Bythrow, P.F., and Potemra, T.A.: Birkeland currents and energetic particles associated with optical auroral signatures of a westward traveling surge, *J. Geophys. Res.*, 92, 8691–8699, 1987.

Chertok, I.M., Belov, A.V., and Abunin, A.A.: Solar eruptions, Forbush decreases, and geomagnetic disturbances from outstanding active region 12673, *Space Weather*, 16, 1549–1560, doi:10.1029/2018SW001899, 2018.

30 Christiansen, F.; Papitashvili, V. O.; Neubert, T., Seasonal variations of high-latitude field-aligned currents inferred from Ørsted and Magsat observations, *J. Geophys. Res.*, 107, SMP 5-1, doi:10.1029/2001JA900104, 2002.

Clilverd, M.A., Rodger, C.J., Brundell, J.B., Dalzell, M., Martin, I., Mac Manus, D.H., et al.: Long-lasting geomagnetically induced currents and harmonic distortion observed in New Zealand during the 7–8 September 2017 disturbed period, *Space Weather*, 16, 704–717, doi:10.1029/2018SW001822, 2018.

Coxon, J.C., Milan, S.E., Clausen, L.B.N., Anderson, B.J., and Korth, H.: A superposed epoch analysis of the regions 5 1 and 2 Birkeland currents observed by AMPERE during substorms, *J. Geophys. Res.: Space Phys.*, 119, 9834–9846, doi:10.1002/2014JA020500, 2014.

Cowley, S.W.H.: Magnetosphere-ionosphere interactions: A tutorial review, in *Magnetospheric Current Systems*, *Geophys. Monogr. Ser.*, 118, 91–106, AGU, Washington, D. C., 2000.

Curto, J.J., Marsal, S., Blanch, E., and Altadill, D.: Analysis of the solar flare effects of 6 September 2017 in the 10 ionosphere and in the Earth's magnetic field using spherical elementary current systems, *Space Weather*, 16, doi:10.1029/2018SW001927, 2018.

Dungey, J.W.: Interplanetary magnetic fields and the auroral zones, *Phys. Rev. Lett.*, 6, 47–48, doi:10.1103/PhysRevLett.6.47, 1961.

Dunlop, M. W., Yang, Y.-Y., Yang J.-Y., Lühr, H., Shen, C., et al.: Multispacecraft current estimates at swarm, J. 15 *Geophys. Res. Space Phys.*, 120, doi:10.1002/2015JA021707. 2015.

Elphic, R.C., Bonnell, J.W., Strangeway, R.J., Kepko, L., Ergun, R.E., et al.: The auroral current circuit and field-aligned currents observed by FAST, *Geophys. Res. Lett.*, 25, 2033–2036, 1998.

Iijima, T., and Potemra T.A.: The amplitude distribution of field-aligned currents at northern high latitudes observed by Triad, *J. Geophys. Res.*, 81(13), 2165–2174, doi:10.1029/JA081i013p02165, 1976.

Iijima, T., Fujii, R., Potemra, T.A., and Saflekos, N.A.: Field-aligned currents in the south polar cusp and their 20 relationship to the interplanetary magnetic field, *J. Geophys. Res.*, 83, 5595–5603, doi:10.1029/JA083iA12p05595, 1978.

Iijima, T., and Potemra, T.: The amplitude distribution of field-aligned currents associated with substorms, *J. Geophys. Res.*, 83, 599–615, 1978.

Iijima, T., Potemra, T.A., Zanetti, L.J., and Bythrow, P.F.: LargeScale Birkeland Currents in the Dayside Polar 25 Region During Strongly Northward IMF: A New Birkeland Current System, *J. Geophys. Res.*, 89, 7441–7452, doi:10.1029/JA089iA09p07441, 1984.

Janhunen, P., Olsson, A., Amm, O., and Kauristie, K.: Characteristics of a stable arc based on FAST and MIRACLE observations, *Ann. Geophys.*, 18, 152–160, 2000.

Johnson, M.L., Murphree, J.S., Marklund, G.T., and Karlsson, T.: Progress on relating optical auroral forms and electric field patterns, *J. Geophys. Res.*, 103, 4271–4284, doi:10.1029/97JA00854, 1998.

Juusola, L., Kauristie, K., Vanhamaki, H., Aikio, A., and van de Kamp M.: Comparison of auroral ionospheric and field-aligned currents derived from Swarm and ground magnetic field measurements, *J. Geophys. Res. Space Phys.*, 121, 9256–9283, doi:10.1002/2016JA022961, 2016.

5 Friis-Christensen, E., Luhr, H., Knudsen, D., and Haagmans, R., Swarm—An Earth observation mission investigating geospace, *Adv. Space Res.*, 41(1), 210–216, 2008.

Fukunishi, H., Fujii, R., Kokubun, S., Tohyama, F., Mukai T., and Oya H.: Small-scale field-aligned currents observed by the Akebono (EXOS-D) satellite, *Geophys. Res. Lett.*, doi:10.1029/91GL00036, 1991.

Ganushkina, N.Y., Liemohn, M.W., Dubyagin, S., Daglis, I.A., Dandouras, I., et al.: Defining and resolving current systems in geospace *Ann. Geophys.*, 33, 1369–1402, doi:10.5194/angeo-33-1369-2015, 2015.

10 Gjerloev, J.W., Ohtani, S., Iijima, T., Anderson, B., Slavin, J., and Le, G.: Characteristics of the terrestrial field-aligned current system *Ann. Geophys.*, 29, 1713–1729, doi:10.5194/angeo-29-1713-2011, 2011.

Green, D.L., Waters, C.L., Anderson, B.J., and Korth, H.: Seasonal and interplanetary magnetic field dependence of the field-aligned currents for both Northern and Southern Hemispheres, *Ann. Geophys.*, 27, 1701–1715, www.ann-geophys.net/27/1701/2009/, 2009.

15 Kozlovsky, A., Aikio, A., Turunen, T., Nilsson, H., Sergienko, T., Safargaleev, V., and Kauristie K.: Dynamics and electric currents of morningside Sun-aligned auroral arcs, *J. Geophys. Res.*, 112, A06306, doi:10.1029/2006JA012244, 2007.

Knudsen, D., Burchill, J.K., Berg, K., et al.: A low energy charged particle distribution imager with a compact sensor for space applications, *Rev. Sci. Instrum.*, 74, 202–211, 2003.

20 Korth, H., Anderson, B. J., and Waters, C. L.: Statistical analysis of the dependence of large-scale Birkeland currents on solar wind parameters, *Ann. Geophys.*, 28, pp. 515–530, doi:10.5194/angeo-28-515-2010, 2010.

Lewis, R.V., Williams, P.J.S., Jones, G.O., Opgenoorth, H.J., and Persson, M.A.L.: The electrodynamics of a drifting auroral arc, *Ann. Geophys.*, 12, 478, 1994.

25 Liemohn, M.W., et al.: Dominant role of the asymmetric ring current in producing the storm-time Dst. *J. Geophys. Res.*, 106, 10883–10904. 2001.

Lui, A.T.Y.: Current disruption in the Earth’s magnetosphere: Observations and models, *J. Geophys. Res.*, 101, 13067–13 088, 1996.

Luhr, H., Park, J., Gjerloev, J.W., Rauberg, J., Michaelis, I., Merayo, J.M.G., and Brauer, P.: Field-aligned currents’ scale analysis performed with the Swarm constellation. *Geophys. Res. Lett.*, 42, 1–8, doi:10.1002/2014GL062453, 2015.

30 Luhr, H., Huang, T., Wing, S., Kervalishvili, G., Rauberg, J., and Korth, H.: Filamentary field-aligned currents at the polar cap region during northward interplanetary magnetic field derived with the Swarm constellation. *Ann. Geophys.*, 34, 901–915, doi:10.5194/angeo-34-901-2016, 2016.

Lukianova, R., and Kozlovsky, A.: Dynamics of polar boundary of the auroral oval derived from the IMAGE satellite data, *Cosmic Res.*, 51(1), 46–53, doi:10.1134/S0010952513010061, 2013.

Lukianova, R.Yu., Kozlovskii, A., and Christiansen F.: field-aligned currents in the winter and summer hemispheres caused by IMF *By*, *Geomag. Aeronomy*, 52(3), 300–308, doi:10.1134/S0016793212020089, 2012.

5 Lyons, L.R.: Formation of auroral arcs via magnetosphere-ionosphere coupling, *Rev. Geophys.*, 30, 93–112, 1992.

Marchaudon, A., Cerisier, J.-C., Greenwald, R.A., and Sofko, G.J.: Electrodynamics of a flux transfer event: Experimental test of the Southwood model, *Geophys. Res. Lett.*, 31, L09809, doi:10.1029/2004GL019922, 2004.

Marchaudon, A., Cerisier, J.-C., Bosqued, J.-M., Owen, C. J., Fazakerley, A. N., and Lahiff, A. D.: On the structure of field-aligned currents in the mid-altitude cusp, *Ann. Geophys.*, 24, 3391-3401, doi:10.5194/angeo-24-3391-2006, 10 2006.

Marklund, G., Sandahl, I., and Opgenoorth, H.: A study of the dynamics of a discrete auroral arc, *Planet. Space Sci.*, 30, 179–197, doi:10.1016/0032-0633(82)90088-5, 1982.

McGranaghan, R.M., Mannucci, A.J., and Forsyth, C.: A comprehensive analysis of multiscale field-aligned currents: Characteristics, controlling parameters, and relationships, *J. Geophys. Res.: Space Phys.*, 122, 11931–11960, 15 doi:10.1002/2017JA024742, 2017.

Merayo, J.G. M., Juergensen, J.L., Friis-Christensen, E., Brauer, P., Primdahl, F., Juergensen, P.S., Allin, T.H. and Denver, T.: The Swarm Magnetometry Package, 143–151, Springer, Dordrecht, Netherlands, doi:10.1007/978-1-4020-6943-7_13, 2008.

Milan, S.E., Cowley, W.H., Lester, M., Wright, D.M., Slavin, J.A., Fillingim, M., Carlson, C. W., and Singer, H.J.: 20 Response of the magnetotail to changes in the open flux content of the magnetosphere, *J. Geophys. Res.*, 109, doi:10.1029/2003JA010350, 2004.

Neubert, T., and Christiansen, F.: Small-scale, field-aligned currents at the top-side ionosphere, *Geophys. Res. Lett.*, 30(19), 2010, doi:10.1029/2003GL017808, 2003.

Opgenoorth, H.J., Haggstrom, I., Williams, P.J.S., and Jones, G.O.L.: Regions of strongly enhanced perpendicular 25 electric fields adjacent to auroral arcs, *J. Atmos. Terr. Phys.*, 52, 449– 458, doi:10.1016/0021-9169(90)90044-N, 1990.

Papitashvili, V.O., Christiansen, F., and Neubert, T.: A new model of field-aligned currents derived from high-precision satellite magnetic field data, *Geophys. Res. Lett.*, 29(14), 1683, doi:10.1029/2001GL014207, 2002.

Pu, Z.Y., Raeder, J., Zhong, J., Bogdanova, Y.V., Dunlop, M., Xiao, C.J., Wang, X.G., and Fazakerley, A.: Magnetic 30 topologies of an in vivo FTE observed by Double Star/TC-1 at Earth's magnetopause, *Geophys. Res. Lett.*, 40, 3502–3506, doi:10.1002/grl.50714, 2013.

Ridley A.J.: Effects of seasonal changes in the ionospheric conductances on magnetospheric field-aligned currents, *Geophys. Res. Lett.* 34, L05101, 2007.

Ritter, P., and Lühr, H.: Curl-B technique applied to Swarm constellation for determining field-aligned currents, *Earth Planets Space*, 58(4), 463-476, 2006.

Ritter, P. and Lühr, H.: Near-Earth magnetic signature of magnetospheric substorms and an improved substorm current model, *Ann. Geophys.*, 26, 2781-2793, doi:10.5194/angeo-26-2781-2008, 2008.

5 Ritter, P., Lühr, H., and Rauberg, J.: Determining field-aligned currents with the Swarm constellation mission, *Earth, Planets and Space*, 65, 1285-1294, doi:10.5047/eps.2013.09.006, 2013.

Swarm Level 2 Processing System Consortium. Detailed Processing Model (DPM) FAC (Tech. Rep. SW-DS-GFZ-GS-0002): Swarm Level 2 Processing System, 2012.

Southwood, D.J.: The ionospheric signature of flux transfer events, *J. Geophys. Res.*, 92, 3207-3213, 1987.

10 Tanskanen, E.I.: A comprehensive high-throughput analysis of substorms observed by IMAGE magnetometer network: Years 1993-2003 examined, *J. Geophys. Res.*, 114, A05204, doi:10.1029/2008JA013682, 2009.

Vennerstrøm, S., Moretto, T., Olsen, N., Friis-Christensen, E., Stampe, A. M., and Watermann, J. F.: Field-aligned currents in the dayside cusp and polar cap region during northward IMF, *J. Geophys. Res.*, 107(A8), doi:10.1029/2001JA009162, 2002.

15 Wang, H., Luhr, H., Ma, S.Y., Weygand, J., Skoug, R.M., and Yin, F.: Field-aligned currents observed by CHAMP during the intense 2003 geomagnetic storm events, *Ann. Geophys.*, 24, 311-324, SRef-ID:1432-0576/ag/2006-24-311, 2006.

Watermann, J., Stauning, P., Lühr, H., Newell, P. T., Christiansen, F., Schlegel, K.: Are small-scale field-aligned currents and magnetosheath-like particle precipitation signatures of the same low-altitude cusp?, *Adv. Space Res.*, 43, 20 41-46, doi: 10.1016/j.asr.2008.03.031, 2009.

Weimer, D.R.: Maps of ionospheric field-aligned currents as a function of the interplanetary magnetic field derived from Dynamics Explorer 2 data, *J. Geophys. Res.*, 106, 2889-12902, 2001.

25 Wu, J., Knudsen, D.J., Gillies, D.M., Donovan, E.F., and Burchill, J.K.: Swarm Observation of Field-Aligned Currents Associated With Multiple Auroral Arc Systems, *J. Geophys. Res.: Space Phys.*, 122, 10145-10156, doi:10.1002/2017JA024439, 2017.

Yasyukevich, Yu., Astafyeva, E., Padokhin, A., Ivanova, V., Syrovatskii, S., and Podlesnyi A.: The 6 September 2017 X-class solar flares and their impacts on the ionosphere, GNSS and HF radio wave propagation, *Space Weather*, 16, doi:10.1029/2018SW001932, 2018.